

---

# PolyMon: A Unified Framework for Polymer Property Prediction

---

**Gaopeng Ren\***  
Department of Chemistry  
Imperial College London

**Yijie Yang\***  
Department of Chemistry  
Imperial College London

**Jiajun Zhou**  
Department of Chemistry  
Imperial College London

**Kim E. Jelfs†**  
Department of Chemistry  
Imperial College London

## Abstract

Accurate prediction of polymer properties is essential for materials design, but remains challenging due to data scarcity, diverse polymer representations, and the lack of systematic evaluation across modelling choices. Here, we present PolyMon, a unified and accessible framework that integrates multiple polymer representations, machine learning methods, and training strategies within a single, accessible platform. PolyMon supports various descriptors and graph construction strategies for polymer representations, and includes a wide range of models, from tabular models to graph neural networks, along with flexible training strategies including multi-fidelity learning,  $\Delta$ -learning, active learning, and ensemble learning. Using five key polymer properties as benchmarks, we perform systematic evaluations to assess how representations and models affect predictive performance. These case studies further illustrate how different training strategies can be applied within a consistent workflow to leverage limited data and incorporate physical model-derived information. Overall, PolyMon provides a comprehensive and extensible foundation for benchmarking and advancing machine learning-based polymer property prediction. The code is available at [github.com/fate1997/polymon](https://github.com/fate1997/polymon).

## 1 Introduction

Polymers underpin a wide range of industrial applications, including therapeutics [1], sensors [2], semiconductors [3], agriculture [4], and energy technologies [5]. Accurate prediction of polymer properties can enable large-scale virtual screening and inverse design. Machine learning (ML) has become an important tool for polymer property prediction [6, 7, 8]. Similar to small organic molecules, polymers can be represented using descriptors, molecular graphs, or sequence-based formats. Descriptor-based methods provide efficient baseline models for polymer property prediction [9, 10, 11]. Graph neural networks (GNNs) have attracted increasing attention for learning representations from molecular graphs and have shown promising performance across a range of polymer properties [12, 13, 14, 15, 16]. Sequence-based representations, such as SMILES strings, further enable large language models to learn transferable polymer representations through unsupervised pretraining on large-scale unlabeled data [17, 18, 19, 20, 21, 22].

Data scarcity remains one of the central challenges in training ML models for polymer property prediction. To mitigate this limitation, a range of training strategies has been proposed, including multi-fidelity learning,  $\Delta$ -learning, active learning, and ensemble learning. Multi-fidelity learning

---

\*Equal contribution

†Corresponding email: [k.jelfs@imperial.ac.uk](mailto:k.jelfs@imperial.ac.uk)

seeks to exploit both high-fidelity experimental data and lower-fidelity computational data [23, 24, 25, 26], which is particularly relevant for polymer systems where experimental measurements are scarce and molecular dynamics (MD) simulations offer a more accessible source of labelled data [27]. Low-fidelity information can be incorporated through techniques such as transfer learning and  $\Delta$ -learning.  $\Delta$ -learning, which aims to learn the residual corrections for labels or embeddings, has gained increasing attention, especially for energy-related properties [28, 29, 30]. From a data-centric perspective, active learning provides an efficient strategy to selectively acquire the most informative data points for improving model performance [31, 32, 33, 34]. Ensemble learning improves robustness by aggregating predictions from multiple models. Despite these advances, systematic investigations into how polymer representations, model architectures, and training strategies jointly influence predictive performance remain limited. Moreover, several recently developed ML techniques, such as TabPFN [35], Kolmogorov-Arnold networks (KANs) [36], and modern  $\Delta$ -learning formulations, are still relatively underexplored in polymer property prediction.

Here, we present PolyMon, a unified and accessible framework that integrates diverse polymer representations, multiple ML models, and flexible training strategies. PolyMon supports polymer featurisation using descriptors from heterogeneous sources as well as molecular graphs constructed with different strategies. The framework incorporates a broad range of ML models, including tabular learners and graph neural networks (GNNs), and further includes recently proposed architectures such as KANs and KAN-based GNNs. In addition, PolyMon provides easy-to-use implementations of advanced training strategies, including multi-fidelity learning,  $\Delta$ -learning, active learning, and ensemble learning. Leveraging this framework, we conduct extensive experiments on polymer property prediction using five key polymer properties as benchmarks.

## 2 Polymer Representations and Models

The overall PolyMon framework is illustrated in Figure 1. PolyMon supports multiple data representations, ML models, and training strategies, and all experiments in this work are conducted using it. Training and evaluation across different data types, models, and strategies can be performed via a single command-line script. The available command arguments and example codes used to generate the results reported here are provided in Section S1 of the Supplementary Information (SI). To ensure fair comparisons between models, we perform hyperparameter optimisation for each model, with the hyperparameter search spaces listed in Section S2 of the SI.

### 2.1 Descriptors and Tabular Models

Polymer descriptors are numerical representations that can be used as input for tabular ML models. Directly calculating descriptors for polymers is often challenging, as the exact degree of polymerisation is typically unknown. Consequently, we focus primarily on descriptors derived from monomers and dimers and use them to approximate polymer representations.

Extended-connectivity fingerprints (ECFPs) [37] are widely used structural descriptors for molecules. These circular topological fingerprints are represented as binary vectors. Here, we use ECFP with a radius of 2 and a length of 2048, referred to as **ECFP4**. The Molecular ACCess System (MACCS) keys [38] are 166-bit binary vectors representing the presence of predefined substructures. Both ECFP and MACCS descriptors are calculated using RDKit [39]. RDKit also provides another predefined descriptor set (**RDKit**) that includes common physicochemical properties (e.g., molecular weight) and structural features (e.g., number of rotatable bonds). We removed descriptors that produced "NaN" or infinite values, yielding a total of 196 usable RDKit descriptors. **Mordred** [40] is a specialised software for descriptor calculation that offers a wide range of structural and property descriptors. After filtering unstable descriptors, we obtained 704 usable Mordred descriptors. As polymers consist of repeating units, descriptors derived from a single monomer may miss information about interactions between units. To capture such information, we also calculated descriptors for dimers, denoted as **ECFP (dimer)**, **RDKit (dimer)**, and **Mordred (dimer)**. Large language models provide an alternative approach for generating polymer representations. Here, we evaluated descriptors from **PolyBERT** [21] and our prior work **PolyCL** [17], both of which were trained on millions of polymers using unsupervised learning, with descriptor vectors of length 600.

With these descriptors, tabular models can be used to fit the data and make predictions. Here, we evaluated several tree-based methods, including random forest (**RF**) [41], **XGBoost** [42], **CatBoost**

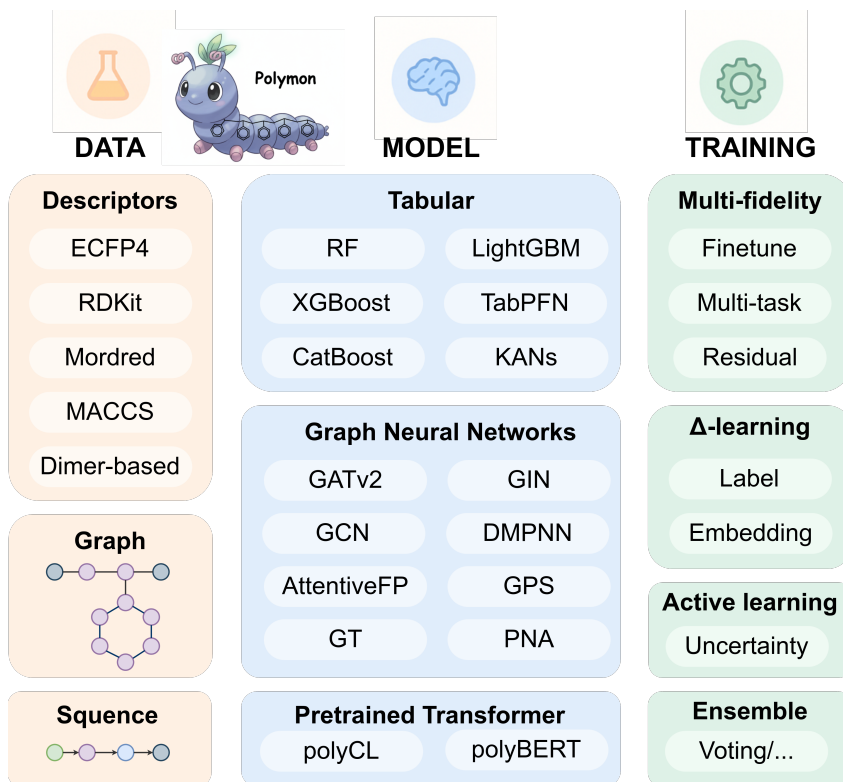


Figure 1: An overview of the PolyMon framework. The framework supports multiple polymer representations, modelling approaches, and training strategies for polymer property prediction. The PolyMon logo was designed with assistance from Gemini.

[43], and **LightGBM** [44]. We also tested a tabular foundation model, **TabPFN** [35], which is pretrained on synthesised tabular datasets. Multi-layer perceptrons (**MLP**) [45], a fundamental module in deep learning, can also be applied to tabular inputs. Recently, Kolmogorov-Arnold Networks (KANs) [36] have emerged as a promising alternative to MLPs. However, the original KANs have a slow training process, making them impractical for datasets with hundreds of descriptors. To address this, we selected several KAN variants with substantially faster training, including **FastKAN** [46], **FourierKAN** [47], and **EfficientKAN** [48].

## 2.2 Graph and GNNs

Molecular graphs can capture intrinsic information about molecular structures. Polymers can be represented using several types of graphs (Figure 2). We considered three graph representations: (i) **monomer graphs**, in which neighbours of attachment points are treated as special atoms; (ii) **periodic graphs**, which introduce a special edge connecting attachment points to capture repeating structures; and (iii) **graphs with virtual nodes**, where a virtual node is added and connected to all other nodes, with the final representation of the graph taken from the virtual node embedding. Unless otherwise noted, we primarily use monomer graphs in this study.

GNNs can be applied to these graphs to iteratively update node (and optionally edge) embeddings through multiple message-passing layers. After node updates, a readout phase typically aggregates the updated node embeddings to construct a graph-level representation, which is then passed to MLPs for property prediction. Here, we evaluated several conventional GNNs, including Graph Convolutional Networks (**GCN**) [49], Graph Attention Networks (**GATv2**) [50], Graph Isomorphism Network (**GIN**) [51], and **AttentiveFP** [52]. We also tested more recent architectures, such as Principal Neighbourhood Aggregation (**PNA**) [53], Graph Transformers (**GT**) [54], and **GPS** [55]. To examine the effect of 3D structural information, we generated monomer conformers by initialising

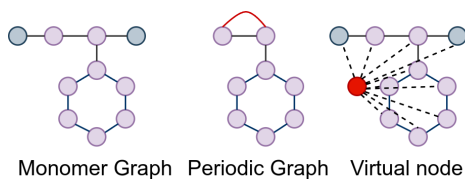


Figure 2: Polymer graphs. Purple nodes denote atoms, blue nodes represent the neighbours of attachment points, and the red node indicates a virtual node. Black edges correspond to chemical bonds, red edges denote additional connections between attachment points, and dashed edges represent virtual connections between atoms and the virtual node.

geometries using ETKDGv3 [56] and optimising them with the MMFF force field [57]. We then applied **DimeNet++** [58], an SE(3)-invariant network, for polymer property prediction.

Recently proposed GNN variants that combine multiple architectures were also evaluated. These include a GATv2 layer followed by a GraphSAGE layer (**GATv2-SAGE**) [12], GATv2 followed by LineEvo layers (**GATv2-LineEvo**) [59], and KAN-based GNNs (**KAN-GCN** and **KAN-GATv2**) [60], where node embedding projections were replaced with Fourier KAN layers. Furthermore, we tested replacing MLPs in GNNs with FastKAN, resulting in **FastKAN-GATv2**, **FastKAN-GIN**, and **FastKAN-GPS**. Detailed information on how KAN is incorporated into GNNs can be found in Section S3.1 of the SI. Finally, we explored GATv2 with different polymer representations: **GATv2-Periodic** for periodic graphs and **GATv2-VN** for graphs with virtual nodes, using RDKit descriptors as the initial embeddings for the virtual nodes.

### 3 Training Strategies

#### 3.1 Multi-fidelity Learning

In polymer property prediction, it is common for datasets to originate from different sources, such as MD simulations or experimental measurements, and exhibit varying fidelities. Here, we explored three strategies for handling multi-fidelity data, using GATv2 as the base model and polymer density prediction as an example task. We used density datasets of different fidelities (MD and experimental data) and evaluated model performance using 5-fold cross-validation on the experimental dataset as the benchmark. We used the following three approaches (detailed information on these multi-fidelity strategies can be found in Section S3.2 of the SI):

- **Finetuning (transfer learning)**: we trained a GATv2 model on the low-fidelity dataset and then finetuned it on the high-fidelity dataset. The polymer representations were either frozen or updated during finetuning, referred to as finetune (freeze) and finetune (all), respectively.
- **Label residual**: we trained a GATv2 model on the low-fidelity dataset, then used a new GATv2 model to predict the residual between the labels estimated by the pretrained model and the ground-truth high-fidelity labels. This approach is referred to as residual (label).
- **Embedding residual**: we trained a GATv2 model on the low-fidelity dataset and extracted the graph embeddings from the pretrained model. A new GATv2 was then trained with these pretrained embeddings added to its graph embeddings. This approach is referred to as residual (emb).

#### 3.2 $\Delta$ -Learning

$\Delta$ -Learning is particularly useful for multi-task and multi-fidelity learning (e.g., the label residual and embedding residual strategies described in Section 3.1).  $\Delta$ -Learning also provides a convenient way to incorporate prior knowledge into GNNs. We evaluated three  $\Delta$ -Learning strategies as follows (detailed information can be found in Section S3.3 of the SI):

- **Property knowledge transfer**: Many polymer properties are correlated. To leverage information from related properties, we incorporated graph embeddings from a GATv2 model pretrained on other properties.

- **Empirical equations:** Certain properties can be roughly estimated using empirical equations. To exploit this prior knowledge, we trained a GATv2 model to predict the residual between the ground-truth labels and the estimates from these equations. For polymer density, we implemented three estimators: a van der Waals-based estimator (vdW), Fedors’ group contribution method (Fedors) [61], and a group contribution method from the IBM GitHub repository (IBM) [62]. For the radius of gyration ( $R_g$ ), we constructed an estimator based on the monomer and a predefined chain length (mono). Additional details are provided in Section S3.3.2 of the SI.
- **Atomic contribution:** Similar to approaches used in energy prediction, simple atomic contribution models can provide rough property estimates based on atom counts. We trained a GATv2 model to learn the residual between the ground-truth labels and these atomic-based estimates.

### 3.3 Active Learning

Using  $R_g$  as the example, we introduce the MD setup and the active learning strategy used here. The initial  $R_g$  dataset was compiled from two prior studies by Hayashi *et al.* [27] and Liu *et al.* [63], both of which reported  $R_g$  values obtained from MD simulations. The dataset from Liu *et al.* [63] contains both labelled and unlabelled polymers. The labelled subset, along with those from Hayashi’s dataset, was used to train the initial model, while the unlabelled subset served as a candidate pool for active learning. Active learning is designed to improve predictive accuracy by selectively sampling new data points that are expected to be most informative. Here, we applied a standard active learning workflow to demonstrate how our unified framework can systematically improve polymer property prediction. The workflow consists of the following steps:

- 1) **Initial training:** A GATv2 model was trained on the initial labelled dataset. Scaffold-based splitting was used to create training, validation, and test sets, and model hyperparameters were optimised using the validation set. The optimised hyperparameters were fixed and reused throughout all active importing cycles. The scaffold-based test set was held out and used only for evaluation during the active learning process.
- 2) **Data acquisition:** Two acquisition strategies were compared: uncertainty-based sampling and random sampling. For uncertainty-based sampling, a model was trained using 5-fold cross-validation on the combination of the training set and validation set and then used to predict  $R_g$  values for all unlabelled monomers. Prediction uncertainty was quantified as the standard deviation of  $R_g$  predictions across the five models. The 100 monomers with the highest uncertainty were selected for labelling. For random sampling, 100 monomers were selected uniformly at random from the unlabelled pool without using a model. All selected monomers were labelled by running new MD simulations.
- 3) **Model retraining:** The newly labelled samples were added to the existing training dataset, and the model was retrained using the same 5-fold cross-validation procedure.
- 4) **Evaluation:** Model performance was evaluated on the fixed hold-out test set from scaffold splitting using mean absolute error (MAE).

Each pass through these steps constitutes one active learning round. The process was repeated for six rounds, resulting in a total of 600 newly labelled and unique monomers. MD simulations were performed with RadonPy[27] to generate labels for selected monomers. Further details are in Section S3.4 of the SI.

### 3.4 Ensemble Learning

Ensemble learning is a common strategy for improving predictive accuracy and robustness by combining multiple models rather than relying on a single predictor. PolyMon incorporates several ensemble learning strategies to systematically assess their impact on polymer property prediction. Specifically, we implemented **voting**, **bagging**, **gradient boosting**[64], **snapshot**[65], and **soft gradient boosting**[66], following standard formulations adapted from the TorchEnsemble GitHub repository[67]. These methods are supported within the same training and evaluation pipeline, enabling direct comparison with non-ensemble models.  $R_g$  was used as a representative case to demonstrate the utility of ensemble learning. Ensemble models were trained on the same initial

scaffold-split dataset used in the active learning experiments, while evaluation was performed on the corresponding hold-out test set using MAE. To examine the effect of ensemble size, we considered four numbers of base estimators, including 5, 10, 15, and 20, for each ensemble method. For reference, a single model trained without ensembling was included as a baseline. All models, both with and without ensembles, were trained using identical hyperparameters to ensure a fair comparison.

## 4 Results and discussion

### 4.1 Datasets and metrics

We investigated different methods for predicting five polymer properties: glass transition temperature ( $T_g$ ), fractional free volume (FFV), thermal conductivity (TC), density, and radius of gyration ( $R_g$ ). These properties are critical for various polymer applications, including as membranes and electrolytes. As summarised in Table 1, most datasets contained over one thousand entries. The  $T_g$  and  $\rho_{\text{exp}}$  datasets are experimentally measured, while the remaining datasets (FFV, Tc,  $R_g$ , and  $\rho_{\text{md}}$ ) are derived from MD simulations.

Table 1: Dataset summary

Dataset	Description	Unit	# data points	Source
$T_g$	Glass transition temperature	°C	7,367	[68]
FFV	Fractional free volume	1	7,030	[63]
TC	Thermal conductivity	W/(m · K)	1,070	[27]
$\rho_{\text{md}}$	MD-calculated density	g/cm <sup>3</sup>	1,077	[27]
$R_g$	Radius of gyration	Å	1,328	[27, 63]
$\rho_{\text{exp}}$	Experimentally measured density	g/cm <sup>3</sup>	117	[69]

We used  $T_g$ , FFV, TC,  $\rho_{\text{md}}$ , and  $R_g$  to evaluate the performance of descriptor-based tabular models, graph-based GNNs, and  $\Delta$ -learning approaches. MAE was employed as the primary metric for comparing different methods across datasets. The datasets  $\rho_{\text{exp}}$  and  $\rho_{\text{md}}$  were used to assess the performance of various multi-fidelity training strategies. To reduce the influence of dataset splitting, we report the mean MAE over 5-fold cross-validation as the final performance. Additionally, we used the weighted MAE (wMAE) [63] to quantify overall performance across the five properties. The wMAE is calculated as:

$$\text{wMAE} = \frac{1}{|\mathcal{X}|} \sum_{X \in \mathcal{X}} \sum_{i \in \mathcal{J}(X)} \omega_i \cdot |\hat{y}_i(X) - y_i(X)|, \quad (4.1)$$

where  $\mathcal{X}$  is the set of polymers being evaluated, and  $\mathcal{J}(X)$  is the property sets for polymer  $X$ . The terms  $\hat{y}_i(X)$  and  $y_i(X)$  are the predicted label and ground truth label for the  $i$ -th property of polymer  $X$ . The weights  $w_i$  for different properties are calculated by:

$$w_i = \frac{1}{(y_i^{\text{max}} - y_i^{\text{min}})} \cdot \frac{K \cdot \sqrt{1/n_i}}{\sum_{j=1}^K \sqrt{1/n_j}}, \quad (4.2)$$

where  $n_i$  is the number of data points for the  $i$ -th property, and  $K$  is the number of property sets ( $K = 5$  in this work). For active learning and ensemble learning, we kept a hold-out test set and used the MAE on the test set as the performance.

### 4.2 The performance of tabular models

We first evaluated various tabular models using RDKit descriptors. As shown in Table 2, TabPFN emerged as the top performer, achieving the lowest wMAE of 0.0228 and consistently delivering the best results across all individual properties. Benefiting from pretraining on millions of synthetic datasets, TabPFN effectively captures both property–feature relationships and inter-feature dependencies. The KAN variants, specifically FastKAN and EfficientKAN, ranked as the second-best architectures, outperforming MLP and traditional tree-based models such as RF and XGBoost. Owing

Table 2: MAE of tabular models using RDKit descriptors (lower is better). Note that bold values indicate the best-performing models; underlined values indicate the second best.

Model	$\rho_{\text{md}}$	FFV	$R_g$	TC	$T_g$	wMAE
TabPFN	<b>0.0121</b> $\pm 0.0012$	<b>0.0053</b> $\pm 0.0003$	<b>2.0015</b> $\pm 0.1536$	<b>0.0171</b> $\pm 0.0004$	<b>23.5880</b> $\pm 0.1705$	<b>0.0228</b>
FastKAN	<u>0.0146</u> $\pm 0.0010$	<u>0.0061</u> $\pm 0.0002$	2.2862 $\pm 0.1948$	0.0214 $\pm 0.0027$	26.2204 $\pm 1.0159$	<u>0.0271</u>
EfficientKAN	0.0167 $\pm 0.0014$	0.0066 $\pm 0.0001$	<u>2.2535</u> $\pm 0.2179$	<u>0.0211</u> $\pm 0.0019$	28.7122 $\pm 1.1073$	0.0279
MLP	0.0149 $\pm 0.0010$	0.0065 $\pm 0.0001$	2.3959 $\pm 0.02641$	<u>0.0211</u> $\pm 0.0012$	29.0279 $\pm 0.7730$	0.0279
LightGBM	0.0223 $\pm 0.0031$	0.0067 $\pm 0.0004$	2.4571 $\pm 0.0969$	0.0216 $\pm 0.0011$	25.3985 $\pm 0.3770$	0.0295
CatBoost	0.0229 $\pm 0.0033$	<u>0.0061</u> $\pm 0.0005$	2.3854 $\pm 0.1789$	0.0228 $\pm 0.0008$	25.9516 $\pm 0.4698$	0.0300
RF	0.0273 $\pm 0.0043$	0.0073 $\pm 0.0004$	2.4820 $\pm 0.1760$	0.0239 $\pm 0.0012$	28.1031 $\pm 0.4177$	0.0325
XGBoost	0.0283 $\pm 0.0040$	0.0071 $\pm 0.0004$	3.4709 $\pm 0.1709$	0.0235 $\pm 0.0014$	33.3332 $\pm 0.4230$	0.0365
FourierKAN	0.0597 $\pm 0.0050$	0.0108 $\pm 0.0003$	3.1513 $\pm 0.2595$	0.0296 $\pm 0.0022$	36.9348 $\pm 1.1130$	0.0472

to their learnable activation functions, KANs possess stronger expressive capacity than standard MLPs.

We further evaluated the impact of different molecular descriptors using an RF baseline (Table 3). Both Mordred (dimer) and standard Mordred descriptors achieved the highest predictive accuracy, with wMAEs of 0.0286 and 0.0294, respectively. RDKit (dimer) and standard RDKit descriptors yielded the second-best performance. Mordred and RDKit offer a diverse set of descriptors, including functional group counts, topological features, and estimated properties, which collectively help tabular models capture the structure-property relationships. Interestingly, descriptors computed on dimers often perform as well as, or better than, those computed on monomers. This improvement is to be expected and likely arises because dimers encode additional information, including the inter-monomer relationships. Notably, while the ECFP4 fingerprint is generally less effective for most thermodynamic properties, it delivered the best prediction for the radius of gyration ( $R_g = 2.289 \pm 0.124$ ), highlighting that the structural connectivity captured by fingerprints is particularly relevant for polymer chain dimensions. Pretrained embeddings from language models (PolyCL and PolyBERT), on the other hand, did not outperform the conventional descriptors. These embeddings are obtained through self-supervised learning on chemical structures; however, their non-end-to-end nature may limit their task-specific performance. We also evaluated other combinations of models and descriptors, with the results presented in Section S4.1 of the SI.

Table 3: MAE of RF models with different descriptors (lower is better). Note that bold values indicate the best-performing descriptors; underlined values indicate the second best.

Descriptor	$\rho_{\text{md}}$	FFV	$R_g$	TC	$T_g$	wMAE
Mordred (dimer)	<b>0.0203</b> $\pm 0.0019$	<b>0.0071</b> $\pm 0.0004$	<u>2.2941</u> $\pm 0.1957$	<b>0.0213</b> $\pm 0.0013$	<b>25.9871</b> $\pm 0.4465$	<b>0.0286</b>
Mordred	<u>0.0202</u> $\pm 0.0025$	<b>0.0071</b> $\pm 0.0004$	2.3571 $\pm 0.1424$	<u>0.0224</u> $\pm 0.0014$	<u>26.7003</u> $\pm 0.4835$	<u>0.0294</u>
RDKit (dimer)	0.0276 $\pm 0.0035$	<u>0.0073</u> $\pm 0.0004$	2.4329 $\pm 0.1873$	0.0235 $\pm 0.0009$	27.3671 $\pm 0.3136$	0.0321
RDKit	0.0273 $\pm 0.0043$	<u>0.0073</u> $\pm 0.0004$	2.4820 $\pm 0.1760$	0.0239 $\pm 0.0012$	28.1031 $\pm 0.4177$	0.0325
MACCS	0.0347 $\pm 0.0056$	0.0087 $\pm 0.0003$	2.5062 $\pm 0.1838$	0.0255 $\pm 0.0007$	28.5440 $\pm 0.7880$	0.0355
ECFP4	0.0434 $\pm 0.0046$	0.0085 $\pm 0.0004$	<b>2.2886</b> $\pm 0.1243$	0.0242 $\pm 0.0005$	28.3704 $\pm 0.6550$	0.0360
ECFP4 (dimer)	0.0443 $\pm 0.0040$	0.0087 $\pm 0.0004$	2.3258 $\pm 0.1686$	0.0245 $\pm 0.0011$	28.7794 $\pm 0.8403$	0.0366
PolyCL	0.0456 $\pm 0.0023$	0.0091 $\pm 0.0005$	2.5627 $\pm 0.2454$	0.0263 $\pm 0.0021$	31.9435 $\pm 0.9320$	0.0392
PolyBERT	0.0483 $\pm 0.0033$	0.0099 $\pm 0.0005$	2.4666 $\pm 0.1639$	0.0252 $\pm 0.0015$	33.1941 $\pm 0.5011$	0.0393

### 4.3 Performance of GNNs

We evaluated the performance of different GNN architectures for polymer property prediction (Table 4). Among the tested models, the PNA network achieved the best overall performance with a wMAE of 0.0193. The GPS architecture also showed highly competitive results, particularly for predicting  $T_g$  and  $R_g$ . GPS combines a global attention layer (graph transformer) to capture long-range interactions with a local message-passing layer for short-range interactions, which likely contributes to its strong performance. The GT model also performed well, highlighting the importance of incorporating long-range interactions in polymer property prediction.

Other classic GNNs, including GCN, GATv2, AttentiveFP, and GIN, maintained high accuracy, demonstrating the effectiveness of graph-based representations in capturing complex structure-

property relationships. Conversely, the KAN- and FastKAN-based GNNs did not outperform their standard counterparts, suggesting that further careful network design is required to fully leverage the potential of KAN architectures. Moreover, although 3D structural information is generally important for polymer properties, DimeNet++ performed poorly, likely because the force-field-generated monomer structures were insufficiently accurate.

We also tested two GATv2 variants augmented with GraphSAGE and LineEvo layers. Both variants outperformed the vanilla GATv2, consistent with findings reported in [12, 59]. This improvement may result from neighbour sampling in GraphSAGE and the inclusion of coarse-grained information in LineEvo. Regarding graph construction strategies, periodic graphs outperformed monomer graphs, likely because they allow message passing between attachment sites. In contrast, GATv2-VN (graphs with virtual nodes) underperformed relative to the other representations, especially for  $T_g$ , showing larger errors and standard deviations. We also tested three additional GNNs on certain tasks, including two novel methods proposed in this work. These models either underperformed relative to the baseline or could not complete within the specified time; their performance is therefore reported in Section S4.2 of the SI.

To compare the performance of GNNs with tabular models, we evaluated TabPFN and LightGBM using Mordred (dimer) descriptors and compared them with PNA and GPS. As shown in Figure 3, for most properties except density, PNA and GPS outperform TabPFN and LightGBM. Interestingly, TabPFN achieves comparable or even superior performance to some GNNs, highlighting that descriptor-based tabular models remain competitive for polymer property prediction.

Table 4: MAE of deep learning models on polymer properties (lower is better). Note that bold values indicate the best-performing models; underlined values indicate the second best.

Model	$\rho_{md}$	FFV	$R_g$	TC	$T_g$	wMAE
PNA	<u>0.0129</u> $\pm 0.0008$	<b>0.0043</b> $\pm 0.0002$	<u>1.5583</u> $\pm 0.1598$	<b>0.0134</b> $\pm 0.0017$	22.1203 $\pm 0.7736$	<b>0.0193</b>
GPS	0.0143 $\pm 0.0009$	<u>0.0044</u> $\pm 0.0002$	<b>1.5377</b> $\pm 0.1242$	0.0151 $\pm 0.0017$	<b>21.8669</b> $\pm 1.0246$	<u>0.0204</u>
GCN	0.0122 $\pm 0.0004$	0.0046 $\pm 0.0002$	1.7321 $\pm 0.1783$	0.0155 $\pm 0.0016$	<u>21.9623</u> $\pm 1.0744$	0.0208
AttentiveFP	0.0122 $\pm 0.0007$	0.0046 $\pm 0.0001$	1.6858 $\pm 0.1368$	0.0162 $\pm 0.0021$	22.8237 $\pm 1.1944$	0.0211
GT	0.0124 $\pm 0.0008$	0.0045 $\pm 0.0002$	1.8355 $\pm 0.1740$	0.0158 $\pm 0.0015$	22.0453 $\pm 0.6657$	0.0213
GIN	0.0139 $\pm 0.0016$	0.0047 $\pm 0.0002$	1.6918 $\pm 0.1640$	0.0174 $\pm 0.0021$	23.1889 $\pm 0.5599$	0.0222
FastKAN-GPS	0.0162 $\pm 0.0020$	0.0047 $\pm 0.0002$	1.7733 $\pm 0.2368$	0.0185 $\pm 0.0025$	<u>22.0537</u> $\pm 0.6651$	0.0234
KAN-GCN	0.0173 $\pm 0.0016$	0.0075 $\pm 0.0027$	1.7718 $\pm 0.1600$	0.0163 $\pm 0.0014$	25.7657 $\pm 0.9712$	0.0237
DimetNet++	0.0266 $\pm 0.0014$	0.0085 $\pm 0.0006$	1.8707 $\pm 0.1656$	0.0216 $\pm 0.0015$	30.5145 $\pm 1.1085$	0.0298
FastKAN-GIN	0.0328 $\pm 0.0025$	0.0060 $\pm 0.0006$	3.2891 $\pm 0.4014$	0.0290 $\pm 0.0113$	41.2818 $\pm 2.0626$	0.0409
GATv2-SAGE	<b>0.0121</b> $\pm 0.0006$	0.0048 $\pm 0.0004$	1.6249 $\pm 0.0863$	0.0156 $\pm 0.0008$	22.4938 $\pm 0.9094$	0.0206
GATv2-LineEvo	0.0130 $\pm 0.0006$	0.0048 $\pm 0.0001$	1.6383 $\pm 0.1731$	<u>0.0150</u> $\pm 0.0019$	23.3476 $\pm 0.4781$	0.0207
GATv2	0.0136 $\pm 0.0005$	0.0046 $\pm 0.0001$	1.7065 $\pm 0.0711$	0.0172 $\pm 0.0007$	22.4999 $\pm 0.7899$	0.0220
FastKAN-GATv2	0.0138 $\pm 0.0012$	0.0048 $\pm 0.0002$	1.7733 $\pm 0.1565$	0.0163 $\pm 0.0015$	24.8758 $\pm 1.0911$	0.0222
KAN-GATv2	0.0195 $\pm 0.0067$	0.0066 $\pm 0.0001$	1.7889 $\pm 0.1724$	0.0161 $\pm 0.0009$	25.2952 $\pm 1.1712$	0.0239
GATv2-Periodic	0.0143 $\pm 0.0023$	0.0047 $\pm 0.0002$	1.6690 $\pm 0.1459$	0.0155 $\pm 0.0017$	23.3959 $\pm 0.8349$	0.0213
GATv2-VN	0.0162 $\pm 0.0009$	0.0049 $\pm 0.0002$	2.4094 $\pm 0.2087$	0.0213 $\pm 0.0020$	58.8836 $\pm 31.6556$	0.0330

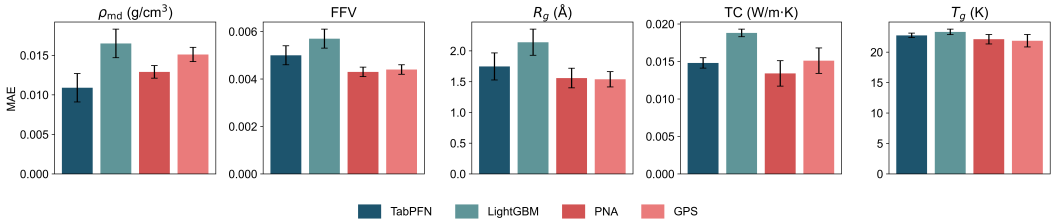


Figure 3: Performance comparison between tabular models (TabPFN and LightGBM) and GNNs (PNA and GPS) on five polymer properties.

#### 4.4 The performance of different training strategies

As shown in Fig. 4a, we evaluated the performance of different strategies for the multi-fidelity task on the density property. All strategies achieved better performance than the baseline, which corresponds to a GATv2 trained directly on  $\rho_{\text{exp}}$ . For the finetuning strategy, we tested two cases: freezing the GNN layers and training only the prediction head (finetune (freeze)) and training all parameters during finetuning (finetune (all)). Both approaches achieved similar performance, with finetune (freeze) performing slightly better, likely due to reduced forgetting compared to finetune (all). For the residual strategy, we compared learning the residual at the label level (residual (label)) versus the embedding level (residual (emb)). We found that using the estimated labels from the low-fidelity model provides more improvement for the high-fidelity model than using the low-fidelity embeddings. In particular, the label residual strategy improved performance by over 10% relative to the baseline model.

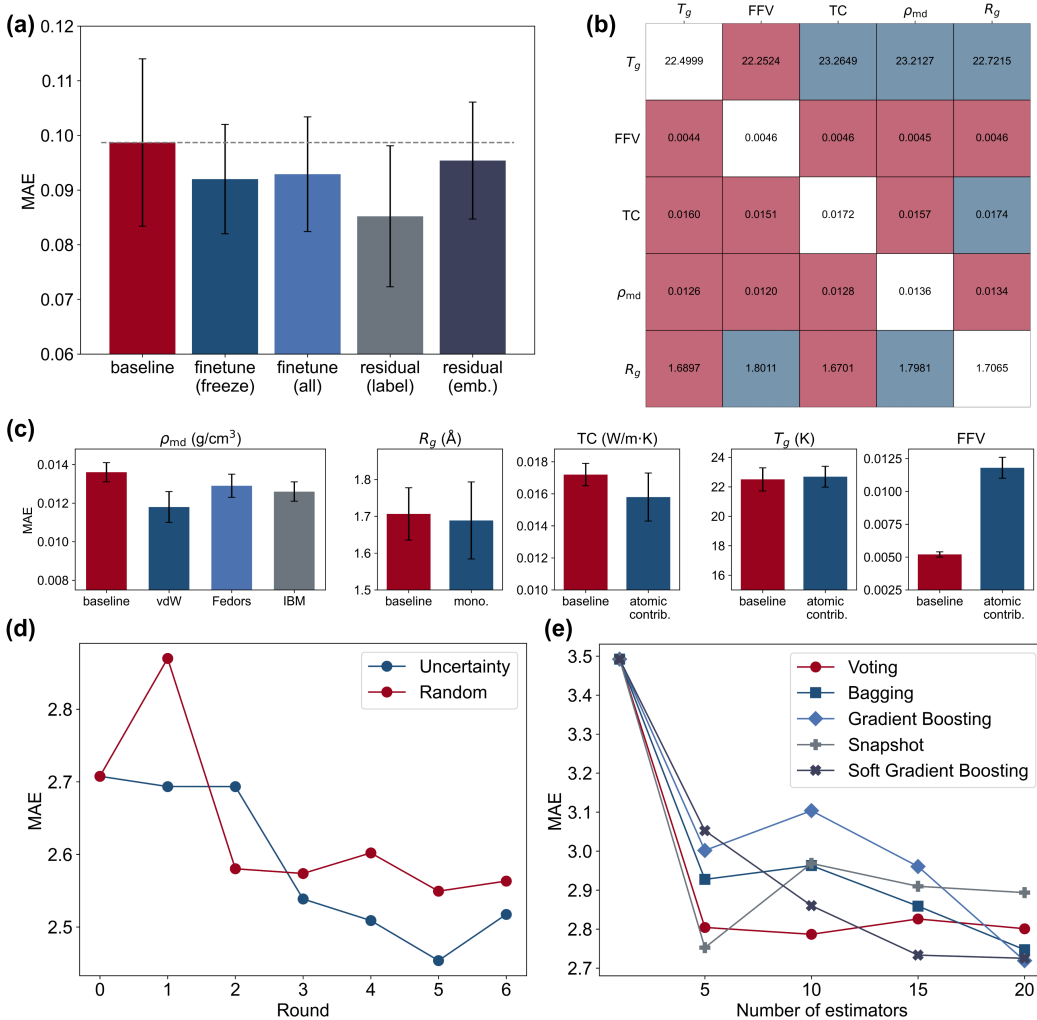


Figure 4: Performance of different training strategies. (a) Multi-fidelity learning on the experimental density dataset ( $\rho_{\text{exp}}$ ); baseline: GATv2 trained directly on  $\rho_{\text{exp}}$ . **finetune (freeze/all)**: pretrained on  $\rho_{\text{md}}$  then finetuned on  $\rho_{\text{exp}}$ , with frozen or fully trainable parameters. **residual (label/emb)**: residual learning on labels or graph embeddings. (b) Property knowledge transfer: each row shows the target property using embeddings from the column property. Diagonal: baseline; red: improved, blue: worse. (c)  $\Delta$ -learning using empirical equations ( $\rho_{\text{md}}$ ,  $R_g$ ) or atomic contributions (TC,  $T_g$ , FFV). (d) Active learning: "Random" selects points randomly; "Uncertainty" selects based on uncertainty. (e) Ensemble performance with varying numbers of estimators.

$\Delta$ -learning has been widely used for training ML force fields [70]. Here, we found that it can also improve performance in polymer property prediction (Figs. 4b and c). The performance matrix for the property knowledge transfer strategy shows that the prediction of one property can be enhanced by incorporating graph embeddings from other properties, particularly for the TC,  $\rho_{\text{md}}$ , and  $R_g$  datasets. These datasets are relatively small compared to  $T_g$  and FFV, and can benefit from the inductive bias provided by related properties. This demonstrates that property knowledge transfer can effectively mitigate data scarcity for certain polymer properties.  $\Delta$ -learning on labels is another effective strategy to introduce inductive bias or reduce training difficulty. As shown in Fig. 4c, all density estimation methods improved performance relative to the baseline, with the vdW-based estimator achieving the best results. Interestingly, although the vdW-based estimator does not provide more accurate estimates than the two other group contribution-based methods (Figure S1), it helps GNNs achieve better performance. This may be because the group contribution methods can produce inconsistent estimates when certain functional groups are absent from their predefined sets, reducing stability. In contrast, the simple vdW-based estimator offers consistent and stable predictions, even if it is less accurate than the group contribution methods. Similar trends are observed for  $R_g$ , where the monomer-based estimator (mono.) improves performance compared to the baseline. Atomic contribution methods, however, sometimes degrade performance, as seen for  $T_g$  and FFV. For the TC dataset, the atomic contribution method improves performance by approximately 8%.

Active learning offers a promising approach to improve the performance of property prediction models with high data efficiency. Fig. 4d compares uncertainty-guided data selection (i.e., active learning) with random data selection. By identifying out-of-distribution points, uncertainty-based selection can improve model generalisability and achieve better performance with fewer labelled data compared to random selection. As the number of active learning rounds increases, both strategies show improved performance, highlighting the importance of incorporating additional labelled data. Combining active learning with MD simulations represents a particularly promising direction for polymer property prediction.

Ensemble learning is commonly used to improve predictive performance by training multiple models and aggregating their predictions. The performance of different ensemble strategies is shown in Fig. 4e. In general, most strategies show improved performance as the number of estimators increases. Among the five ensemble strategies tested, we found that the simple voting strategy achieved the best overall performance. Compared to single models, all ensemble methods provided measurable improvements, with the best ensemble model (gradient boosting with 20 estimators) improving performance by over 20%.

## 5 Conclusion

We have developed **PolyMon**, a unified framework for polymer property prediction. PolyMon supports a range of data representations, from conventional descriptors to graph structures, and integrates diverse ML models, including tabular models, GNNs, and novel variants. Unlike other property prediction frameworks, PolyMon also incorporates flexible training strategies, such as multi-fidelity learning,  $\Delta$ -learning, active learning, and ensemble learning. Using five representative polymer properties  $T_g$ , TC, FFV, density, and  $R_g$ , we conducted comprehensive benchmarks to evaluate the performance of different models and strategies. Overall, GNNs generally outperform tabular models, though carefully designed descriptors allow tabular models to achieve comparable results in some cases. Experiments with different training strategies further demonstrate their effectiveness in improving predictive accuracy. PolyMon provides a flexible, efficient, and user-friendly platform for conducting such experiments and can serve as a foundation for advancing ML-driven polymer design in the future (the code can be found at <https://github.com/fate1997/polymon>).

## Author contributions

G.R. and Y.Y. developed the framework, conducted experiments, and analysed the results. J.Z. contributed to project conceptualisation and expertise in pre-trained polymer language models. K.E.J. supervised the project. G.R. and Y.Y. drafted the manuscript, and all authors contributed to the final version.

## Conflicts of interest

There are no conflicts of interest to declare.

## Data availability

All the data, code and models used to generate the results are available in the Github repository at [github.com/fate1997/polymon](https://github.com/fate1997/polymon).

## Acknowledgements

G.R. acknowledge Imperial College London for funding through the President’s PhD Scholarship. K.E.J. acknowledges the AI for Chemistry: Alchemy hub for funding (EPSRC grant EP/Y028775/1 and EP/Y028759/1). We thank the organisers of the “NeurIPS – Open Polymer Prediction 2025” Kaggle competition for providing the polymer datasets and inspiring this work.

## References

- [1] Rainer Haag and Felix Kratz. Polymer Therapeutics: Concepts and Applications. *Angew. Chemie Int. Ed.*, 45(8):1198–1215, 2006.
- [2] Basudam Adhikari and Sarmishtha Majumdar. Polymers in sensor applications. *Prog. Polym. Sci.*, 29(7):699–766, 2004.
- [3] Li Ding, Zi-Di Yu, Xiao-Ye Wang, Ze-Fan Yao, Yang Lu, Chi-Yuan Yang, Jie-Yu Wang, and Jian Pei. Polymer semiconductors: synthesis, processing, and applications. *Chem. Rev.*, 123(12):7421–7497, 2023.
- [4] Lubhan Cherwoo, Ishika Gupta, Ranjana Bhatia, and Hema Setia. Improving agricultural practices: application of polymers in agriculture. *Energy, Ecol. Environ.*, 9(1):25–41, 2024.
- [5] Saswata Bose, Tapas Kuila, Thi Xuan Hien Nguyen, Nam Hoon Kim, Kin Tak Lau, and Joong Hee Lee. Polymer membranes for high temperature proton exchange membrane fuel cell: Recent advances and challenges. *Prog. Polym. Sci.*, 36(6):813–843, 2011.
- [6] Lei Tao, Vikas Varshney, and Ying Li. Benchmarking machine learning models for polymer informatics: an example of glass transition temperature. *J. Chem. Inf. Model.*, 61(11):5395–5413, 2021.
- [7] Tarak K Patra. Data-Driven Methods for Accelerating Polymer Design. *ACS Polym. Au*, 2(1):8–26, 2022.
- [8] Cheng Yan and Guoqiang Li. The Rise of Machine Learning in Polymer Discovery. *Adv. Intell. Syst.*, 5(4):2200243, 2023.
- [9] Nilay K Roy, Walter D Potter, and David P Landau. Polymer property prediction and optimization using neural networks. *IEEE Trans. Neural Netw. Learn. Syst.*, 17(4):1001–1014, 2006.
- [10] Yuankai Zhao, Roger J Mulder, Shadi Houshyar, and Tu C Le. A review on the application of molecular descriptors and machine learning in polymer design. *Polym. Chem.*, 14(29):3325–3346, 2023.
- [11] Gabriel Bradford, Jeffrey Lopez, Jurgis Ruza, Michael A Stolberg, Richard Osterude, Jeremiah A Johnson, Rafael Gomez-Bombarelli, and Yang Shao-Horn. Chemistry-informed machine learning for polymer electrolyte discovery. *ACS Cent. Sci.*, 9(2):206–216, 2023.
- [12] Owen Queen, Gavin A McCarver, Saitheeraj Thatigotla, Brendan P Abolins, Cameron L Brown, Vasileios Maroulas, and Konstantinos D Vogiatzis. Polymer graph neural networks for multitask property learning. *npj Comput. Mater.*, 9(1):90, 2023.
- [13] Matteo Aldeghi and Connor W Coley. A graph representation of molecular ensembles for polymer property prediction. *Chem. Sci.*, 13(35):10486–10498, 2022.

- [14] Jaehong Park, Youngseon Shim, Franklin Lee, Aravind Rammohan, Sushmit Goyal, Munbo Shim, Changwook Jeong, and Dae Sin Kim. Prediction and Interpretation of Polymer Properties Using the Graph Convolutional Network. *ACS Polym. Au*, 2(4):213–222, 2022.
- [15] Evan R Antoniuk, Peggy Li, Bhavya Kailkhura, and Anna M Hiszpanski. Representing polymers as periodic graphs with learned descriptors for accurate polymer property predictions. *J. Chem. Inf. Model.*, 62(22):5435–5445, 2022.
- [16] Rishi Gurnani, Christopher Kuenneth, Aubrey Toland, and Rampi Ramprasad. Polymer Informatics at Scale with Multitask Graph Neural Networks. *Chem. Mater.*, 35(4):1560–1567, 2023.
- [17] Jiajun Zhou, Yijie Yang, Austin M Mroz, and Kim E Jelfs. PolyCL: contrastive learning for polymer representation learning via explicit and implicit augmentations. *Digit. Discov.*, 4(1):149–160, 2025.
- [18] Seunghye Han, Yeonghun Kang, Hyunsoo Park, Jeesung Yi, Geunyeong Park, and Jihan Kim. Multimodal transformer for property prediction in polymers. *ACS Appl. Mater. Interfaces*, 16(13):16853–16860, 2024.
- [19] Haoke Qiu, Luniang Liu, Xuepeng Qiu, Xuemin Dai, Xiangling Ji, and Zhao-Yan Sun. PolyNC: a natural and chemical language model for the prediction of unified polymer properties. *Chem. Sci.*, 15(2):534–544, 2024.
- [20] Changwen Xu, Yuyang Wang, and Amir Barati Farimani. TransPolymer: a Transformer-based language model for polymer property predictions. *npj Comput. Mater.*, 9(1):64, 2023.
- [21] Christopher Kuenneth and Rampi Ramprasad. polyBERT: a chemical language model to enable fully machine-driven ultrafast polymer informatics. *Nat. Commun.*, 14(1):4099, 2023.
- [22] Ning Liu, Siavash Jafarzadeh, Brian Y Lattimer, Shuna Ni, Jim Lua, and Yue Yu. Harnessing large language models for data-scarce learning of polymer properties. *Nat. Comput. Sci.*, 5(3):245–254, 2025.
- [23] Abhirup Patra, Rohit Batra, Anand Chandrasekaran, Chiho Kim, Tran Doan Huan, and Rampi Ramprasad. A multi-fidelity information-fusion approach to machine learn and predict polymer bandgap. *Comput. Mater. Sci.*, 172:109286, 2020.
- [24] Clyde Fare, Peter Fenner, Matthew Benatan, Alessandro Varsi, and Edward O Pyzer-Knapp. A multi-fidelity machine learning approach to high throughput materials screening. *npj Comput. Mater.*, 8(1):257, 2022.
- [25] David Buterez, Jon Paul Janet, Steven J Kiddle, Dino Oglic, and Pietro Lió. Transfer learning with graph neural networks for improved molecular property prediction in the multi-fidelity setting. *Nat. Commun.*, 15(1):1517, 2024.
- [26] Tsz Wai Ko and Shyue Ping Ong. Data-efficient construction of high-fidelity graph deep learning interatomic potentials. *npj Comput. Mater.*, 11(1):65, 2025.
- [27] Yoshihiro Hayashi, Junichiro Shiomi, Junko Morikawa, and Ryo Yoshida. RadonPy: automated physical property calculation using all-atom classical molecular dynamics simulations for polymer informatics. *npj Comput. Mater.*, 8(1):222, 2022.
- [28] Raghunathan Ramakrishnan, Pavlo O Dral, Matthias Rupp, and O Anatole von Lilienfeld. Big data meets quantum chemistry approximations: the  $\Delta$ -machine learning approach. *J. Chem. Theory Comput.*, 11(5):2087–2096, 2015.
- [29] Lin Shen, Jingheng Wu, and Weitao Yang. Multiscale quantum mechanics/molecular mechanics simulations with neural networks. *J. Chem. Theory Comput.*, 12(10):4934–4946, 2016.
- [30] Yaohuang Huang, Yi-Fan Hou, and Pavlo O Dral. Active delta-learning for fast construction of interatomic potentials and stable molecular dynamics simulations. *Mach. Learn. Sci. Technol.*, 6(3):35004, 2025.
- [31] Renzheng Zhang, Jiabin Xu, Hanfeng Zhang, Guoyue Xu, and Tengfei Luo. Active learning-guided exploration of thermally conductive polymers under strain. *Digit. Discov.*, 4(3):812–823, 2025.
- [32] Jiabin Xu and Tengfei Luo. Unlocking enhanced thermal conductivity in polymer blends through active learning. *npj Comput. Mater.*, 10(1):74, 2024.

- [33] Kevin Maik Jablonka, Giriprasad Melpatti Jothiappan, Shefang Wang, Berend Smit, and Brian Yoo. Bias free multiobjective active learning for materials design and discovery. *Nat. Commun.*, 12(1):2312, 2021.
- [34] Ashna Jose, Emilie Devijver, Noel Jakse, and Roberta Poloni. Informative Training Data for Efficient Property Prediction in Metal–Organic Frameworks by Active Learning. *J. Am. Chem. Soc.*, 146(9):6134–6144, 2024.
- [35] Noah Hollmann, Samuel Müller, Lennart Purucker, Arjun Krishnakumar, Max Körfer, Shi Bin Hoo, Robin Tibor Schirremeister, and Frank Hutter. Accurate predictions on small data with a tabular foundation model. *Nature*, 637(8045):319–326, 2025.
- [36] Ziming Liu, Yixuan Wang, Sachin Vaidya, Fabian Ruehle, James Halverson, Marin Soljagic, Thomas Y. Hou, and Max Tegmark. KAN: Kolmogorov–arnold networks. In *International Conference on Learning Representations*, 2025.
- [37] David Rogers and Mathew Hahn. Extended-connectivity fingerprints. *J. Chem. Inf. Model.*, 50(5):742–754, 2010.
- [38] Joseph L Durant, Burton A Leland, Douglas R Henry, and James G Nourse. Reoptimization of MDL keys for use in drug discovery. *J. Chem. Inf. Comput. Sci.*, 42(6):1273–1280, 2002.
- [39] RDKit: Open-source cheminformatics. <http://www.rdkit.org>. [Online; accessed 11-April-2024].
- [40] Hirotomo Moriwaki, Yu-Shi Tian, Norihito Kawashita, and Tatsuya Takagi. Mordred: a molecular descriptor calculator. *J. Cheminform.*, 10(1):4, 2018.
- [41] Leo Breiman. Random forests. *Mach. Learn.*, 45(1):5–32, 2001.
- [42] Tianqi Chen and Carlos Guestrin. XGBoost: A scalable tree boosting system. In *Proceedings of the 22nd ACM SIGKDD International Conference on Knowledge Discovery and Data Mining*, 2016.
- [43] Liudmila Prokhorenkova, Gleb Gusev, Aleksandr Vorobev, Anna Veronika Dorogush, and Andrey Gulin. CatBoost: unbiased boosting with categorical features. In *Advances in Neural Information Processing Systems*, 2018.
- [44] Guolin Ke, Qi Meng, Thomas Finley, Taifeng Wang, Wei Chen, Weidong Ma, Qiwei Ye, and Tie Yan Liu. LightGBM: A highly efficient gradient boosting decision tree. In *Advances in Neural Information Processing Systems*, 2017.
- [45] Kurt Hornik, Maxwell Stinchcombe, and Halbert White. Multilayer feedforward networks are universal approximators. *Neural Netw.*, 2(5):359–366, 1989.
- [46] Ziyao Li. Kolmogorov-arnold networks are radial basis function networks, 2024.
- [47] Jinfeng Xu, Zheyu Chen, Jinze Li, Shuo Yang, Wei Wang, Xiping Hu, and Edith C-H Ngai. Fourierkan-gcf: Fourier kolmogorov-arnold network—an effective and efficient feature transformation for graph collaborative filtering. *arXiv preprint arXiv:2406.01034*, 2024.
- [48] Blealtan. efficient-kan. <https://github.com/Blealtan/efficient-kan>, 2024.
- [49] Thomas N. Kipf and Max Welling. Semi-supervised classification with graph convolutional networks. In *International Conference on Learning Representations*, 2017.
- [50] Shaked Brody, Uri Alon, and Eran Yahav. How attentive are graph attention networks? In *International Conference on Learning Representations*, 2022.
- [51] Keyulu Xu, Weihua Hu, Jure Leskovec, and Stefanie Jegelka. How powerful are graph neural networks? In *International Conference on Learning Representations*, 2019.
- [52] Zhaoping Xiong, Dingyan Wang, Xiaohong Liu, Feisheng Zhong, Xiaozhe Wan, Xutong Li, Zhaojun Li, Xiaomin Luo, Kaixian Chen, Hualiang Jiang, and Mingyue Zheng. Pushing the boundaries of molecular representation for drug discovery with the graph attention mechanism. *J. Med. Chem.*, 63(16):8749–8760, 2020.
- [53] Gabriele Corso, Luca Cavalleri, Dominique Beaini, Pietro Liò, and Petar Veličković. Principal neighbourhood aggregation for graph nets. In *Advances in Neural Information Processing Systems*, 2020.

- [54] Yunsheng Shi, Zhengjie Huang, Shikun Feng, Hui Zhong, Wenjing Wang, and Yu Sun. Masked label prediction: unified message passing model for semi-supervised classification. In *International Joint Conference on Artificial Intelligence*, 2021.
- [55] Ladislav Rampásek, Mikhail Galkin, Vijay Prakash Dwivedi, Anh Tuan Luu, Guy Wolf, and Dominique Beaini. Recipe for a general, powerful, scalable graph transformer. In *Advances in Neural Information Processing Systems*, volume 35, 2022.
- [56] Shuzhe Wang, Jagna Witek, Gregory A Landrum, and Sereina Riniker. Improving conformer generation for small rings and macrocycles based on distance geometry and experimental torsional-angle preferences. *J. Chem. Inf. Model.*, 60(4):2044–2058, 2020.
- [57] Thomas A Halgren. Merck molecular force field. I. Basis, form, scope, parameterization, and performance of MMFF94. *J. Comput. Chem.*, 17(5-6):490–519, 1996.
- [58] Johannes Gasteiger, Shankari Giri, Johannes T. Margraf, and Stephan Günnemann. Fast and uncertainty-aware directional message passing for non-equilibrium molecules. In *Machine Learning for Molecules Workshop, NeurIPS*, 2020.
- [59] Gao-Peng Ren, Ke-Jun Wu, and Yuchen He. Enhancing molecular representations via graph transformation layers. *J. Chem. Inf. Model.*, 63(9):2679–2688, 2023.
- [60] Longlong Li, Yipeng Zhang, Guanghui Wang, and Kelin Xia. Kolmogorov–Arnold graph neural networks for molecular property prediction. *Nat. Mach. Intell.*, 7(8):1346–1354, 2025.
- [61] R F Fedors. A method to estimate critical volumes. *AIChE J.*, 25(1):202, 1979.
- [62] IBM. polymer\_property\_prediction: A python library for prediction of polymeric material properties. [https://github.com/IBM/polymer\\_property\\_prediction](https://github.com/IBM/polymer_property_prediction), 2024. GitHub repository (archived).
- [63] Gang Liu, Jiaxin Xu, Eric Inae, Yihan Zhu, Ying Li, Tengfei Luo, Meng Jiang, Yao Yan, Walter Reade, Sohier Dane, Addison Howard, and María Cruz. Neurips - open polymer prediction 2025. <https://kaggle.com/competitions/neurips-open-polymer-prediction-2025>, 2025. Kaggle.
- [64] Jerome H. Friedman. Greedy function approximation: A gradient boosting machine. *Ann. Stat.*, 29:1189–1232, 2000.
- [65] Gao Huang, Yixuan Li, Geoff Pleiss, Zhuang Liu, John E Hopcroft, and Kilian Q Weinberger. Snapshot ensembles: Train 1, get m for free. In *International Conference on Learning Representations*, 2017.
- [66] Ji Feng, Yi-Xuan Xu, Yuan Jiang, and Zhi-Hua Zhou. Soft gradient boosting machine. *arXiv preprint arXiv:2006.04059*, 2020.
- [67] TorchEnsemble-Community. Ensemble-pytorch: A unified ensemble framework for pytorch. <https://github.com/TorchEnsemble-Community/Ensemble-Pytorch>, 2024. GitHub repository.
- [68] Sreekanth Kunchapu and Kevin Maik Jablonka. Polymetrix: an ecosystem for digital polymer chemistry. *npj Comput. Mater.*, 11(1):312, 2025.
- [69] Mohammad Atif Faiz Afzal, Andrea R Browning, Alexander Goldberg, Mathew D Halls, Jacob L Gavartin, Tsuguo Morisato, Thomas F Hughes, David J Giesen, and Joseph E Goose. High-throughput molecular dynamics simulations and validation of thermophysical properties of polymers for various applications. *ACS Appl. Polym. Mater.*, 3(2):620–630, 2021.
- [70] Joel M. Bowman, Chen Qu, Riccardo Conte, Apurba Nandi, Paul L. Houston, and Qi Yu. Delta-machine learned potential energy surfaces and force fields. *J. Chem. Theory Comput.*, 19(1):1–17, 2023.

**Supporting Information:**

**PolyMon: A Unified Framework for Polymer  
Property Prediction**

Gaopeng Ren<sup>†</sup>, Yijie Yang<sup>†</sup>, Jiajun Zhou, and Kim E. Jelfs\*

*Department of Chemistry, Molecular Sciences Research Hub, Imperial College London,  
White City Campus, Wood Lane, London, W12 0BZ, U.K.*

E-mail: [k.jelfs@imperial.ac.uk](mailto:k.jelfs@imperial.ac.uk)

# Contents

<b>S1 Program details</b>	<b>S-4</b>
S1.1 Arguments, descriptors, and models . . . . .	S-4
S1.2 Example commands for training tabular models . . . . .	S-8
S1.3 Example commands for training neural networks . . . . .	S-9
S1.4 Example commands for different training strategies . . . . .	S-10
S1.4.1 Multi-fidelity learning . . . . .	S-10
S1.4.2 $\Delta$ -learning . . . . .	S-11
S1.4.3 Active learning . . . . .	S-13
S1.4.4 Ensemble learning . . . . .	S-13
S1.5 Example commands for training different graphs . . . . .	S-14
S1.6 Example Code for Inference . . . . .	S-15
<b>S2 Hyperparameter tuning</b>	<b>S-16</b>
S2.1 Hyperparameter for tabular models . . . . .	S-16
S2.2 Hyperparameter for GNN models . . . . .	S-19
<b>S3 Additional model details</b>	<b>S-23</b>
S3.1 KAN-based GNNs . . . . .	S-23
S3.2 Multi-fidelity learning . . . . .	S-23
S3.3 $\Delta$ -learning . . . . .	S-24
S3.3.1 Property knowledge transfer . . . . .	S-24
S3.3.2 Empirical equations . . . . .	S-24
S3.3.3 Atomic contribution . . . . .	S-26
S3.4 Active learning . . . . .	S-26
<b>S4 Additional results</b>	<b>S-28</b>
S4.1 Full results of tabular models on different descriptors . . . . .	S-28

S4.2 Attempts on other models . . . . . S-30  
S4.3 Performance of empirical equations and atomic contributions . . . . . S-32

**References** **S-33**

## S1 Program details

### S1.1 Arguments, descriptors, and models

Table S1: Arguments for the `polymon train` command.

Argument	Type	Description
<code>--raw-csv</code>	str	Path to the raw CSV file. The CSV file should contain the SMILES column
<code>--sources</code>	str (multiple)	Sources to use for training (only when the input CSV file contains the Source column.)
<code>--tag</code>	str	Tag to use for training.
<code>--labels</code>	str (multiple)	Labels to be predict. The available choice is from the CSV columns.
<code>--feature-names</code>	str (multiple)	Feature names to use for training. Available features can be found in Table S2.
<code>--n-trials</code>	int	Number of trials for hyperparameter optimisation.
<code>--out-dir</code>	str	Output directory.
<code>--hparams-from</code>	str	Path to hyperparameter file (.json, .pt, .pkl).
<code>--n-fold</code>	int	Number of cross-validation folds.
<code>--split-mode</code>	str	Data split mode (random, scaffold).
<code>--seed</code>	int	Random seed.
<code>--remove-hydrogens</code>	bool	Whether to remove hydrogens from molecules.
<code>--descriptors</code>	str (multiple)	Descriptors for training neural network models.
<code>--model</code>	str	Model type. Available models are shown in Table S3.
<code>--hidden-dim</code>	int	Hidden dimension size.
<code>--num-layers</code>	int	Number of model layers.
<code>--batch-size</code>	int	Training batch size.
<code>--lr</code>	float	Learning rate.
<code>--num-epochs</code>	int	Number of training epochs.
<code>--early-stopping-patience</code>	int	Early stopping patience.
<code>--device</code>	str	Training device.
<code>--run-production</code>	bool	Force 0.95:0.05:0.0 train:val:test split.
<code>--finetune</code>	bool	Whether to finetune the model.
<code>--finetune-csv-path</code>	str	CSV file for finetuning.
<code>--pretrained-model</code>	str	Path to pretrained model.
<code>--n-estimator</code>	int	Number of estimators.
<code>--additional-features</code>	str (multiple)	Additional training features.
<code>--skip-train</code>	bool	Skip training step.
<code>--low-fidelity-model</code>	str	Path to low-fidelity model.
<code>--estimator-name</code>	str	Estimator name for base predictions.
<code>--emb-model</code>	str	Model path to provide base graph embeddings.
<code>--ensemble-type</code>	str	Ensemble method.
<code>--train-residual</code>	bool	Label residual.
<code>--normalizer-type</code>	str	Normalization type (normalizer, log_normalizer, none).
<code>--augmentation</code>	bool	Use data augmentation.

Table S2: Available feature names in PolyMon

<b>Descriptor Name</b>	<b>Description</b>
xenonpy_atom	XenonPy atom features
cgcnn	CGCNN atom features
source	Source labels as features
z	Atomic numbers as integers
edge	Default edge features ( <b>bond</b> )
bond	Chemical bond features
fully_connected_edges	Fully connected edge indices
periodic_bond	Add bonds between attachment points to the chemical bonds
virtual_bond	Add a virtual node and bonds connected to other nodes
pos	3D coordinates
relative_position	The relative position of the atom to the nearest attachment
seq	SMILES sequence features
desc	Default descriptor features ( <b>rdkit2d</b> )
rdkit2d	RDKit 2D descriptors
ecfp4	ECFP4 fingerprints
rdkit3d	RDKit 3D descriptors
mordred	Mordred descriptors
maccs	MACCS keys
oligomer_rdkit2d	RDKit 2D descriptors of the oligomer (default is dimer)
oligomer_mordred	Mordred descriptors of the oligomer (default is dimer)
oligomer_ecfp4	ECFP4 fingerprints of the oligomer (default is dimer)
xenonpy_desc	XenonPy composition descriptors
mordred3d	Mordred 3D descriptors
fedors_density	Estimated density from Fedors method
monomer	Monomer without attachment points
polycl	Pretrained Polycl embeddings
polybert	Pretrained PolyBERT embeddings
gaff2_mod	Pretrained GAFF2 descriptors

Table S3: Available models in PolyMon.

Model Type	Model Name	Description
GNNs	gatv2	Graph Attention Network v2
	attentivefp	AttentiveFP
	dimenetpp	DimeNet++
	gatv2vn	GATv2 with virtual node
	gin	Graph Isomorphism Network
	pna	Principal Neighbourhood Aggregation
	gvp	Geometric Vector Perceptron
	gatv2chainreadout	GATv2 with chain readout
	gt	Graph Transformer
	kan_gatv2	KAN-augmented GATv2
	gps	Graph GPS
	kan_gps	KAN-augmented GraphGPS
	fastkan_gatv2	FastKAN-augmented GATv2
	gatv2_lineevo	GATv2 with line evolution
	gatv2_sage	GATv2 with SAGE aggregation
	gatv2_source	GATv2 for multi-fidelity/source
	gatv2_pe	GATv2 with position encoding
	gatv2_embed_residual	GATv2 with embedding residuals
	kan_gin	KAN-augmented GIN
	fastkan_gin	FastKAN-augmented GIN
kan_gcn	KAN-augmented GCN	
dmpnn	Directed Message Passing Neural Network	
kan_dmpnn	KAN-augmented DMPNN	
Tabular	fastkan	Fast KAN for descriptors
	efficientkan	Efficient KAN for descriptors
	fourierkan	Fourier KAN for descriptors
	random_forest	Random Forest model for tabular data
	xgb	XGBoost model for tabular data
	lgbm	LightGBM model for tabular data
	catboost	CatBoost model for tabular data
	tabpfn	TabPFN model for tabular data

## S1.2 Example commands for training tabular models

Hyperparameter optimisation:

```
polymon train \  
  --raw-csv ./database/database.csv \  
  --sources Kaggle PI1070 PolyMetriX \  
  --labels Tg Tc FFV Density Rg \  
  --feature-names rdkit2d \  
  --model rf \  
  --n-fold 5 \  
  --n-trials 15 \  
  --out-dir ./results \  
  --tag debug
```

Hyperparameters from a file:

```
polymon train \  
  --raw-csv ./database/database.csv \  
  --labels Rg \  
  --feature-names ecfp4 \  
  --model rf \  
  --n-fold 5 \  
  --hparams-from ./results/rf/rf-Rg-ecfp4.pkl\  
  --out-dir ./results \  
  --tag debug
```

## S1.3 Example commands for training neural networks

Hyperparameter optimisation:

```
polymon train \  
  --raw-csv ./database/database.csv \  
  --sources Kaggle PI1070 PolyMetriX \  
  --labels Tc Tg FFV Density Rg \  
  --model gatv2 \  
  --n-trials 15 \  
  --n-fold 5 \  
  --out-dir ./results \  
  --tag debug \  
  --num-epochs 2500 \  
  --early-stopping-patience 250
```

Hyperparameters from a file:

```
polymon train \  
  --raw-csv ./database/database.csv \  
  --tag debug \  
  --labels Rg \  
  --model gatv2 \  
  --n-fold 5 \  
  --hparams-from ./results/gatv2/Rg/paper/hparams_opt/hparams.json \  
  --out-dir ./results
```

## S1.4 Example commands for different training strategies

### S1.4.1 Multi-fidelity learning

Finetune the prediction head:

```
polymon train \  
  --tag finetune \  
  --labels Density \  
  --model gatv2 \  
  --n-fold 5 \  
  --finetune \  
  --finetune-csv-path database/database.csv \  
  --sources MAFA-exp \  
  --pretrained-model ./results/gatv2/Density/gatv2_Density_pretrained.pt \  
  --hparams-from ./results/gatv2/Density/hparams.json
```

Label residual:

```
polymon train \  
  --tag label-residual \  
  --labels Density \  
  --model gatv2 \  
  --n-fold 5 \  
  --train-residual \  
  --sources MAFA-exp \  
  --low-fidelity-model ./results/gatv2/Density/gatv2_Density_pretrained.pt \  
  --hparams-from ./results/gatv2/Density/hparams.json
```

## Embedding residual:

```
polymon train \  
  --tag emb-residual \  
  --labels Density \  
  --model gatv2_embed_residual \  
  --n-fold 5 \  
  --sources MAFA-exp \  
  --emb-model ./results/gatv2/Density/gatv2_Density_pretrained.pt \  
  --hparams-from ./results/gatv2/Density/hparams.json
```

### S1.4.2 $\Delta$ -learning

#### Property knowledge transfer:

```
polymon train \  
  --tag from-Tc \  
  --labels Density \  
  --model gatv2_embed_residual \  
  --n-fold 5 \  
  --sources PI1070 Kaggle PolyMetriX \  
  --emb-model ./results/gatv2/Tc/gatv2_Tc_paper.pt \  
  --hparams-from ./results/gatv2/Density/hparams.json
```

### Empirical equations:

```
polymon train \  
  --tag ibm \  
  --labels Density \  
  --model gatv2 \  
  --n-fold 5 \  
  --train-residual \  
  --sources PI1070 Kaggle PolyMetriX \  
  --estimator-name Density-IBM \  
  --hparams-from ./results/gatv2/Density/hparams.json
```

### Atomic contributions:

```
polymon train \  
  --tag residual \  
  --labels FFV \  
  --model gatv2 \  
  --n-fold 5 \  
  --train-residual \  
  --sources PI1070 Kaggle PolyMetriX \  
  --hparams-from ./results/gatv2/FFV/hparams.json
```

### S1.4.3 Active learning

Data acquisition:

```
polymon rec \  
  --pool-csv ./database/raw_csv/JCIM_sup_bigsmiles.csv \  
  --trained-model results/mlp/Rg/paper/mlp_Rg_paper-KFold.pt \  
  --acquisition uncertainty \  
  --save-path debug.csv \  
  --sample-size 20
```

### S1.4.4 Ensemble learning

```
polymon train \  
  --raw-csv ./database/Rg_base.csv \  
  --sources Kaggle PI1070 \  
  --labels Rg \  
  --model gatv2 \  
  --hparams-from ./hparams.json \  
  --n-estimators 10 \  
  --ensemble-type voting \  
  --skip-train \  
  --run-production \  
  --tag voting
```

## S1.5 Example commands for training different graphs

Periodic graph:

```
polymon train \  
  --raw-csv ./database/database.csv \  
  --sources Kaggle PI1070 PolyMetriX \  
  --labels Tc Tg FFV Density Rg \  
  --model gatv2 \  
  --n-fold 5 \  
  --n-trials 15 \  
  --out-dir ./results \  
  --tag periodic \  
  --additional-features monomer periodic_bond
```

Graphs with virtual nodes:

```
polymon train \  
  --raw-csv ./database/database.csv \  
  --labels Rg \  
  --sources PI1070 Kaggle PolyMetriX \  
  --model gatv2vn \  
  --n-fold 5 \  
  --descriptors rdkit2d \  
  --out-dir ./results \  
  --tag debug
```

## S1.6 Example Code for Inference

After training is complete, the output folder may contain three types of model checkpoints: the single model, the K-fold model (filename ending with `KFold.pt`), and the ensemble model (filename ending with `ensemble.pt`). Each saved checkpoint includes all the information required for inference, such as model hyperparameters, model parameters, feature names, normalization parameters, and, if applicable, transformation arguments. Consequently, these models can be loaded and used for prediction directly and effortlessly.

### Single model & K-fold model:

```
from polymon.model.base import ModelWrapper

model = ModelWrapper.from_file('results/mlp/Rg/paper/mlp_Rg_paper-KFold.pt')
# The output shape will be [N, 1] for single models, and [N, k] for k-fold models.
predictions = model.predict(['*C*', '*CCC*'])
```

### Ensemble model:

```
from polymon.model.ensemble import EnsembleModelWrapper

model_path = 'results/gatv2/Rg/bagging/ensemble/production/gatv2_Rg-ensemble.pt'
model = EnsembleModelWrapper.from_file(model_path)
predictions = model.predict(['*C*', '*CC*'])
```

## S2 Hyperparameter tuning

The model was trained using five-fold cross-validation, with hyperparameter optimisation performed using Optuna<sup>1</sup> over a total of 15 trials. The maximum number of training epochs was set to 2000, and early stopping based on validation loss was applied to prevent overfitting. Learning rate is set between  $10^{-4}$  and  $2 \times 10^{-3}$  at a logarithmic scale.

### S2.1 Hyperparameter for tabular models

Table S4: Hyperparameter search space for XGBoost.

Hyperparameter	Description	Search Space
<code>n_estimators</code>	Number of estimators	1000
<code>learning_rate</code>	Boosting learning rate	log-uniform ( $10^{-3}, 10^{-1}$ )
<code>max_depth</code>	Maximum tree depth	Integer [1, 10]
<code>subsample</code>	Row subsampling ratio	Uniform (0.05, 1.0)
<code>colsample_bytree</code>	Feature subsampling ratio	Uniform (0.05, 1.0)
<code>min_child_weight</code>	Minimum child weight	Integer [1, 20]

Table S5: Hyperparameter search space for Random Forest.

Hyperparameter	Description	Search Space
<code>n_estimators</code>	Number of trees	Integer [100, 1000]
<code>max_depth</code>	Maximum tree depth	Integer [2, 32]
<code>min_samples_split</code>	Minimum samples required to split a node	Integer [2, 10]
<code>min_samples_leaf</code>	Minimum samples required at a leaf	Integer [1, 10]

<sup>1</sup><https://github.com/optuna/optuna>

Table S6: Hyperparameter search space for LightGBM.

Hyperparameter	Description	Search Space
<code>n_estimators</code>	Number of estimators	Integer [1000, 10000]
<code>learning_rate</code>	Boosting learning rate	{0.006, 0.008, 0.01, 0.014, 0.017, 0.02}
<code>max_depth</code>	Maximum tree depth	10, 20, 100
<code>num_leaves</code>	Number of leaves	Integer [1, 1000]
<code>reg_alpha</code>	L1 regularization strength	log-uniform ( $10^{-3}$ , 10)
<code>reg_lambda</code>	L2 regularization strength	log-uniform ( $10^{-3}$ , 10)
<code>subsample</code>	Row subsampling ratio	{0.4, 0.5, 0.6, 0.7, 0.8, 1.0}
<code>colsample_bytree</code>	Feature subsampling ratio	{0.3, 0.4, 0.5, 0.6, 0.7, 0.8, 0.9, 1.0}
<code>min_child_samples</code>	Minimum data per leaf	Integer [1, 300]
<code>cat_smooth</code>	Minimum of data per categorical group	Integer [1, 100]

Table S7: Hyperparameter search space for CatBoost.

Hyperparameter	Description	Search Space
<code>learning_rate</code>	Learning rate	Discrete grid: [0.001, 0.020] with step 0.001
<code>depth</code>	Tree depth	Integer [9, 15]
<code>l2_leaf_reg</code>	L2 regularization strength	Discrete grid: [1.0, 5.5] with step 0.5
<code>min_child_samples</code>	Minimum samples per leaf	{1, 4, 8, 16, 32}
<code>grow_policy</code>	Tree growing policy	Depthwise
<code>iterations</code>	Number of iterations for training	10000

Table S8: Hyperparameter search space for TabPFN.

Hyperparameter	Description	Search Space
<code>n_estimators</code>	Number of ensemble estimators	Integer [8, 64]
<code>softmax_temperature</code>	Softmax temperature	{0.75, 0.8, 0.85, 0.9, 0.95, 1.0}
<code>average_before_softmax</code>	Logit averaging strategy	{True, False}

Table S9: Hyperparameter search space for FastKAN.

Hyperparameter	Description	Search Space
<code>hidden_dim</code>	Hidden feature dimension	Discrete grid: $[32, 512]$ with step 32
<code>num_layers</code>	Number of hidden layers in the FastKAN network	Integer:[2, 5]
<code>grid_min</code>	Minimum value of the spline grid range	Integer" $[-5.0, -2.0]$
<code>grid_max</code>	Maximum value of the spline grid range	Integer: $[2.0, 5.0]$
<code>num_grids</code>	Number of spline interpolation grids	Discrete grid: $[6, 10]$ with step 2

Table S10: Hyperparameter search space for FourierKAN.

Hyperparameter	Description	Search Space
<code>hidden_dim</code>	Hidden feature dimension	Discrete grid: $[32, 512]$ with step 32
<code>num_layers</code>	Number of hidden layers in the FastKAN network	Integer:[2, 5]

Table S11: Hyperparameter search space for EfficientKAN.

Hyperparameter	Description	Search Space
<code>hidden_dim</code>	Hidden feature dimension	Discrete grid: $[32, 512]$ with step 32
<code>num_layers</code>	Number of hidden layers in the FastKAN network	Integer:[2, 5]

## S2.2 Hyperparameter for GNN models

Table S12: Hyperparameter search space for GATv2.

Hyperparameter	Description	Search Space
<code>hidden_dim</code>	Hidden feature dimension	{16, 32, 48, 64}
<code>num_layers</code>	Number of graph attention layers	Integer [2, 8]
<code>num_heads</code>	Number of attention heads	{4, 8}
<code>pred_hidden_dim</code>	Hidden dimension of the prediction head	Distance grid:[16, 256] with step 16
<code>pred_dropout</code>	Dropout rate in the prediction head	{0.1, 0.2, 0.3, 0.4, 0.5}
<code>pred_layers</code>	Number of layers in the prediction head	{1, 2, 3}

Table S13: Hyperparameter search space for the Graph Isomorphism Network (GIN).

Hyperparameter	Description	Search Space
<code>hidden_dim</code>	Hidden feature dimension	Discrete grid: [16, 256] with step 16
<code>num_layers</code>	Number of GIN layers	{2, 3, 4}
<code>pred_hidden_dim</code>	Hidden dimension of the prediction (readout) head	Discrete grid: [16, 256] with step 16
<code>pred_dropout</code>	Dropout rate applied to the prediction head	{0.0, 0.1, 0.2, 0.3, 0.4, 0.5}
<code>pred_layers</code>	Number of layers in the prediction head	{1, 2, 3}
<code>n_mlp_layers</code>	Number of MLP layers per GIN block	{1, 2, 3}
<code>dropout</code>	Dropout rate applied to node features	{0.0, 0.1, 0.2, 0.3, 0.4, 0.5}

Table S14: Hyperparameter search space for the Graph Convolutional Network (GCN).

Hyperparameter	Description	Search Space
<code>in_channels</code>	Dimension of input node feature vectors	Distance grid: $[16, 256]$ with step 16
<code>hidden_dim</code>	Hidden feature dimension	Discrete grid: $[16, 256]$ with step 16
<code>num_layers</code>	Number of GCN layers	$\{2, 3, 4\}$
<code>dropout</code>	Dropout rate applied to node features	$\{0.0, 0.1, 0.2, 0.3, 0.4, 0.5\}$

Table S15: Hyperparameter search space for PNA.

Hyperparameter	Description	Search Space
<code>hidden_dim</code>	Hidden feature dimension	Discrete grid: $[16, 256]$ with step 16
<code>towers</code>	Number of aggregation towers	$\{1, 2, 4, 8\}$
<code>num_layers</code>	Number of PNA layers	Integer $[2, 4]$
<code>pred_hidden_dim</code>	Hidden dimension of the prediction (readout) head	Discrete grid: $[16, 256]$ with step 16
<code>pred_dropout</code>	Dropout rate applied to the prediction head	$[0.0, 0.1, 0.2, 0.3, 0.4, 0.5]$
<code>pred_layers</code>	Number of layers in the prediction head	$[1, 2, 3]$

Table S16: Hyperparameter search space for DimeNet++.

Hyperparameter	Description	Search Space
<code>hidden_dim</code>	Hidden feature dimension	Discrete grid: [16, 256] with step 16
<code>num_layers</code>	Number of interaction layers	Integer [2, 4]
<code>num_spherical</code>	Number of spherical basis functions	Integer [5, 10]
<code>num_radial</code>	Number of radial basis functions	{4, 6, 8, 10, 12}
<code>cutoff</code>	Distance cutoff for message passing	{2.0, 2.5, 3.0, 3.5, 4.0, 4.5, 5.0}
<code>int_emb_size</code>	Dimension of interaction embedding layers	Discrete grid: [8, 64] with step 8
<code>basis_emb_size</code>	Dimension of basis function embeddings	[4, 8, 12, 16]
<code>out_emb_channels</code>	Dimension of output embedding channels	Discrete grid: [16, 256] with step 16
<code>max_num_neighbors</code>	Maximum number of neighbours considered per node	Discrete grid: [16, 64] with step 1

Table S17: Hyperparameter search space for AttentiveFP.

Hyperparameter	Description	Search Space
<code>in_channels</code>	Dimension of input node feature vectors	Discrete grid: [16, 256] with step 16
<code>hidden_dim</code>	Hidden feature dimension	Discrete grid: [16, 256] with step 16
<code>num_layers</code>	Number of message-passing layers	{1, 2, 3}
<code>num_timesteps</code>	Number of iterative attention refinement steps	{1, 2, 3}

Table S18: Hyperparameter search space for Graph Transformers(GT).

Hyperparameter	Description	Search Space
<code>hidden_dim</code>	Hidden feature dimension	Distance grid:[16, 512] with step 16
<code>num_layers</code>	Number of graph attention layers	Integer [2, 6]
<code>num_heads</code>	Number of attention heads	{4, 8}
<code>pred_hidden_dim</code>	Hidden dimension of the prediction head	Distance grid:[128, 1024] with step 128
<code>pred_dropout</code>	Dropout rate in the prediction head	{0.0, 0.1, 0.2, 0.3, 0.4, 0.5}
<code>pred_layers</code>	Number of layers in the prediction head	{1, 2, 3}

Table S19: Hyperparameter search space for the Graph Positioning System (GPS) model.

Hyperparameter	Description	Search Space
<code>hidden_dim</code>	Hidden feature dimension	Discrete grid: [16, 256] with step 16
<code>num_layers</code>	Number of stacked GPS layers	Discrete grid: [2, 10] with step 1
<code>pe_dim</code>	Dimension of positional encodings	{4, 5, 6, 7, 8}
<code>heads</code>	Number of attention heads in the transformer component	{4, 8}
<code>attn_type</code>	Type of attention mechanism used in GPS	{performer, multihead}
<code>attention_dropout</code>	Dropout probability used inside the attention module	{0.0, 0.1, 0.2, 0.3, 0.4, 0.5}

## S3 Additional model details

### S3.1 KAN-based GNNs

In this work, we implemented KAN-based GNNs using two complementary strategies. The first follows the approach of Li *et al.*,<sup>S1</sup> in which the linear node projection layer is replaced with a Fourier KAN layer.<sup>S2</sup> The second strategy is based on FastKAN,<sup>S3</sup> which can be used as a drop-in replacement for the MLP blocks in several GNN architectures, including GIN,<sup>S4</sup> GPS,<sup>S5</sup> and GATv2.<sup>S6</sup>

### S3.2 Multi-fidelity learning

For multi-fidelity learning, we first optimised the hyperparameters of a GATv2 model on the low-fidelity dataset ( $\rho_{\text{md}}$ ) using 15 optimisation trials with 5-fold cross-validation. The optimised hyperparameters were then used to train a production model, in which the dataset was split into training and validation sets with a 95:5 ratio. This procedure resulted in a single pretrained model for density prediction. Building upon this pretrained model, we explored several multi-fidelity transfer strategies. For fine-tuning, we considered two variants: updating all parameters of the pretrained model (**finetune (all)**) and updating only the parameters of the prediction head while freezing the remaining layers (**finetune (freeze)**).

For the label-residual and embedding-residual strategies, we trained an additional model using the same hyperparameters as the pretrained one. In the label-residual approach, the model was trained to predict the residual between the ground-truth labels and the predictions produced by the pretrained model. In the embedding-residual approach, the graph embeddings generated by the pretrained model were added to the embeddings produced by the current model to guide the learning process.

## S3.3 $\Delta$ -learning

### S3.3.1 Property knowledge transfer

Many polymer properties are correlated through their underlying chemical structure and chain architecture. To explore whether such relationships can be leveraged during model training, we introduced a property knowledge transfer strategy that incorporates information learned from one property into the prediction of another. The core idea is to reuse representations learned from a model trained on a related property and integrate this information into the target property model in a controlled manner.

As a case study, we used thermal conductivity (TC) to assist density prediction. Specifically, a GATv2 model was trained on the TC dataset. The learned polymer embeddings from the pre-trained TC model are then added to the polymer representation learned by the density model through a residual connection. If the embedding dimensions of the two models differ, a linear projection is applied to ensure compatibility before combining the representations. The final prediction is made using the combined representation, which is then passed through an multi-layer perceptron (MLP) prediction head.

This property knowledge transfer strategy is fully supported within the framework and can be applied to any pair of related polymer properties. Its impact on predictive performance is assessed empirically, allowing the framework to systematically examine when and how transferring information across properties is beneficial, neutral, or detrimental.

### S3.3.2 Empirical equations

Empirical equations can provide fast and physically motivated estimates of polymer properties. Instead of learning the target property directly, a model can be trained to learn the difference ( $\Delta$  value) between the empirical estimate and the ground truth value. However, empirical relationships are not universally available for all polymer properties, and their accuracy can vary across chemical spaces. Here, we incorporate empirical equations for two

properties studied in this framework, namely the radius of gyration ( $R_g$ ) and density.

For  $R_g$ , we implemented two empirical estimators that derive polymer size from monomer structure and physical assumptions without generating three-dimensional conformations. Both methods estimate the monomer contour length from the molecular graph using bond length information, followed by a polymer scaling factor based on the degree of polymerisation, characteristic ratio, and solvent condition. The difference lies in how they derive monomer contour length from the whole polymer chain molecule. One implementation approximates the longest backbone path using a depth-first search (DFS) over the molecular graph, while the other formulates the molecule as a weighted graph and estimates the backbone length using graph shortest path analysis in NetworkX<sup>2</sup>. We used the first strategy to generate the results in the main text. The empirical equation of the  $R_g$  is written as

$$\hat{R}_g = \frac{b}{\sqrt{6}} N_K^\nu \quad (1)$$

$$N_K = \frac{L_c}{b} \quad (2)$$

$$L_c = N l_m \quad (3)$$

where  $b$  is the Kuhn length and  $\nu$  is the solvent dependent scaling exponent.  $N_K$  is the number of Kuhn segments,  $L_c$  and  $l_m$  is the polymer chain and monomer contour length respectively.  $N$  is the degree of polymerisation.

For density, we considered three empirical estimation strategies with different levels of chemical detail. The overall idea is to divide the molecular weight of the monomer by its molecular volume. Two methods differ in how the molar volume is computed. The first method estimates the molar volume from the van der Waals volume of constituent atoms combined with a packing coefficient. The second method follows a group contribution approach developed by IBM<sup>3</sup>, where the molar volume is inferred from atom connectivity

---

<sup>2</sup><https://github.com/networkx/networkx>

<sup>3</sup>[https://github.com/IBM/polymer\\_property\\_prediction/tree/main](https://github.com/IBM/polymer_property_prediction/tree/main)

indices and functional group corrections. The third method adopts the Fedors group contribution scheme<sup>4</sup>, which estimates molar volume by summing contributions from atom types, functional groups, bond types and ring structures. Together, these estimators provide complementary baseline predictions for density.

### S3.3.3 Atomic contribution

Atomic contribution models provide a simple and interpretable way to relate polymer composition to material properties. We implemented an atomic contribution approach that estimates a target property as a linear combination of element-specific contributions weighted by their occurrence in the polymer. In this work, this strategy is applied to thermal conductivity and fractional free volume (FFV).

In this formulation, a polymer is represented by its atomic composition vector, where each entry corresponds to the number of atoms of a given element in the polymer repeating unit. The property value is then estimated as the weighted sum of these atomic counts, with the weights representing element-specific contributions. These contributions are obtained by fitting a linear regression model to available labelled data. During training, the coefficients are learned by minimising the error between predicted and reference property values across the training dataset, with no intercept term to ensure the predictions depend solely on atomic composition.

## S3.4 Active learning

MD simulations were performed to generate labels for selected monomers. We used RadonPy,<sup>S7</sup> an automated workflow for all-atom classical MD simulations, to construct amorphous polymer structures from monomer SMILES strings and compute  $R_g$  values. For each monomer, an amorphous cell containing six polymer chains was generated, with each chain comprising approximately 800 atoms. The reported  $R_g$  value was computed from MD trajectories

---

<sup>4</sup><https://github.com/CalebBell/thermo>

using per-chain data output by LAMMPS. Specifically, time-resolved chain-wise  $R_g$  values were generated along with the simulation trajectory. For each saved timestep, the  $R_g$  was evaluated for all polymer chains in the system. To ensure equilibration, only the final 2000 timesteps of each trajectory were considered for analysis. The  $R_g$  was first averaged over time for each individual chain, and the resulting values were then averaged over all chains to obtain a single mean  $R_g$  for the system. Mathematically, this corresponds to

$$\langle R_g \rangle = \frac{1}{N_{chains}} \sum_{c=1}^{N_{chains}} \left( \frac{1}{N_t} \sum_t R_g(t, c) \right) \quad (4)$$

where  $R_g(t, c)$  denotes the radius of gyration of chain  $c$  at timestep  $t$ ,  $N_t$  is the number of timesteps considered, and  $N_{chains}$  is the number of polymer chains in the system.

## **S4 Additional results**

### **S4.1 Full results of tabular models on different descriptors**

Table S20: Prediction performance (mean $\pm$ std) of different models and molecular descriptors.

Model	Descriptor	$\rho_{\text{md}}$	FFV	$R_g$	TC	$T_g$
CatBoost	ECFP4	0.0358 $\pm$ 0.0033	0.0072 $\pm$ 0.0004	2.134 $\pm$ 0.191	0.0214 $\pm$ 0.0012	23.86 $\pm$ 0.30
	MACCS	0.0322 $\pm$ 0.0047	0.0082 $\pm$ 0.0003	2.502 $\pm$ 0.184	0.0243 $\pm$ 0.0011	28.09 $\pm$ 0.70
	Mordred	0.0231 $\pm$ 0.0037	0.0059 $\pm$ 0.0005	2.293 $\pm$ 0.198	0.0199 $\pm$ 0.0007	23.85 $\pm$ 0.47
	Oligomer-ECFP4	0.0372 $\pm$ 0.0039	0.0075 $\pm$ 0.0004	2.234 $\pm$ 0.253	0.0209 $\pm$ 0.0011	24.22 $\pm$ 0.44
	Oligomer-Mordred	0.0212 $\pm$ 0.0037	0.0056 $\pm$ 0.0005	2.334 $\pm$ 0.232	0.0194 $\pm$ 0.0008	23.31 $\pm$ 0.46
	Oligomer-RDKit2D	0.0226 $\pm$ 0.0030	0.0061 $\pm$ 0.0005	2.355 $\pm$ 0.221	0.0213 $\pm$ 0.0009	25.19 $\pm$ 0.42
	PolyBERT	0.0431 $\pm$ 0.0026	0.0078 $\pm$ 0.0005	2.311 $\pm$ 0.147	0.0295 $\pm$ 0.0017	31.70 $\pm$ 0.44
	PolyCL	0.0350 $\pm$ 0.0031	0.0073 $\pm$ 0.0005	2.329 $\pm$ 0.206	0.0226 $\pm$ 0.0025	27.59 $\pm$ 0.82
	RDKit2D	0.0229 $\pm$ 0.0033	0.0061 $\pm$ 0.0005	2.385 $\pm$ 0.179	0.0228 $\pm$ 0.0008	25.95 $\pm$ 0.47
RDKit3D	0.1032 $\pm$ 0.0064	0.0197 $\pm$ 0.0005	3.444 $\pm$ 0.221	0.0354 $\pm$ 0.0013	68.08 $\pm$ 0.86	
LightGBM	ECFP4	0.0349 $\pm$ 0.0041	0.0073 $\pm$ 0.0004	2.311 $\pm$ 0.303	0.0222 $\pm$ 0.0009	23.93 $\pm$ 0.31
	MACCS	0.0387 $\pm$ 0.0056	0.0083 $\pm$ 0.0003	2.545 $\pm$ 0.166	0.0263 $\pm$ 0.0012	30.31 $\pm$ 0.55
	Mordred	0.0189 $\pm$ 0.0023	0.0057 $\pm$ 0.0004	2.287 $\pm$ 0.148	0.0209 $\pm$ 0.0005	23.76 $\pm$ 0.58
	Oligomer-ECFP4	0.0410 $\pm$ 0.0028	0.0083 $\pm$ 0.0004	2.348 $\pm$ 0.270	0.0214 $\pm$ 0.0010	23.79 $\pm$ 0.53
	Oligomer-Mordred	0.0165 $\pm$ 0.0018	0.0057 $\pm$ 0.0004	2.140 $\pm$ 0.212	0.0188 $\pm$ 0.0005	23.32 $\pm$ 0.45
	Oligomer-RDKit2D	0.0215 $\pm$ 0.0031	0.0065 $\pm$ 0.0003	2.453 $\pm$ 0.201	0.0215 $\pm$ 0.0013	24.72 $\pm$ 0.33
	PolyBERT	0.0394 $\pm$ 0.0030	0.0078 $\pm$ 0.0004	2.350 $\pm$ 0.187	0.0223 $\pm$ 0.0009	26.81 $\pm$ 0.12
	PolyCL	0.0342 $\pm$ 0.0022	0.0072 $\pm$ 0.0004	2.411 $\pm$ 0.209	0.0220 $\pm$ 0.0017	26.88 $\pm$ 0.72
	RDKit2D	0.0223 $\pm$ 0.0031	0.0067 $\pm$ 0.0004	2.457 $\pm$ 0.097	0.0216 $\pm$ 0.0011	25.40 $\pm$ 0.38
RDKit3D	0.0969 $\pm$ 0.0067	0.0198 $\pm$ 0.0005	3.561 $\pm$ 0.152	0.0361 $\pm$ 0.0015	68.23 $\pm$ 0.78	
Random Forest	ECFP4	0.0434 $\pm$ 0.0046	0.0085 $\pm$ 0.0004	2.289 $\pm$ 0.124	0.0242 $\pm$ 0.0005	28.37 $\pm$ 0.66
	MACCS	0.0347 $\pm$ 0.0056	0.0087 $\pm$ 0.0003	2.506 $\pm$ 0.184	0.0255 $\pm$ 0.0007	28.54 $\pm$ 0.79
	Mordred	0.0202 $\pm$ 0.0025	0.0071 $\pm$ 0.0004	2.357 $\pm$ 0.142	0.0224 $\pm$ 0.0014	26.70 $\pm$ 0.48
	Oligomer-ECFP4	0.0443 $\pm$ 0.0040	0.0087 $\pm$ 0.0004	2.326 $\pm$ 0.169	0.0245 $\pm$ 0.0011	28.78 $\pm$ 0.84
	Oligomer-Mordred	0.0203 $\pm$ 0.0019	0.0071 $\pm$ 0.0004	2.294 $\pm$ 0.196	0.0213 $\pm$ 0.0013	25.99 $\pm$ 0.45
	Oligomer-RDKit2D	0.0276 $\pm$ 0.0035	0.0073 $\pm$ 0.0004	2.433 $\pm$ 0.187	0.0235 $\pm$ 0.0009	27.37 $\pm$ 0.31
	PolyBERT	0.0483 $\pm$ 0.0033	0.0099 $\pm$ 0.0005	2.467 $\pm$ 0.164	0.0252 $\pm$ 0.0015	33.19 $\pm$ 0.50
	PolyCL	0.0456 $\pm$ 0.0023	0.0091 $\pm$ 0.0005	2.563 $\pm$ 0.245	0.0263 $\pm$ 0.0021	31.94 $\pm$ 0.93
	RDKit2D	0.0273 $\pm$ 0.0043	0.0073 $\pm$ 0.0004	2.482 $\pm$ 0.176	0.0239 $\pm$ 0.0012	28.10 $\pm$ 0.42
RDKit3D	0.1053 $\pm$ 0.0049	0.0195 $\pm$ 0.0005	3.398 $\pm$ 0.178	0.0358 $\pm$ 0.0019	69.06 $\pm$ 0.74	
XGBoost	ECFP4	0.0479 $\pm$ 0.0041	0.0098 $\pm$ 0.0003	2.553 $\pm$ 0.140	0.0282 $\pm$ 0.0018	29.94 $\pm$ 0.63
	MACCS	0.0367 $\pm$ 0.0054	0.0093 $\pm$ 0.0003	3.460 $\pm$ 0.170	0.0258 $\pm$ 0.0012	34.89 $\pm$ 0.62
	Mordred	0.0209 $\pm$ 0.0030	0.0075 $\pm$ 0.0004	2.859 $\pm$ 0.216	0.0227 $\pm$ 0.0010	26.74 $\pm$ 0.45
	Oligomer-ECFP4	0.0441 $\pm$ 0.0039	0.0087 $\pm$ 0.0004	2.639 $\pm$ 0.174	0.0237 $\pm$ 0.0014	40.64 $\pm$ 0.76
	Oligomer-Mordred	0.0593 $\pm$ 0.0043	0.0072 $\pm$ 0.0004	3.598 $\pm$ 0.178	0.0289 $\pm$ 0.0019	34.80 $\pm$ 0.64
	Oligomer-RDKit2D	0.0417 $\pm$ 0.0034	0.0073 $\pm$ 0.0004	2.537 $\pm$ 0.216	0.0239 $\pm$ 0.0010	32.63 $\pm$ 0.41
	PolyBERT	0.0718 $\pm$ 0.0041	0.0101 $\pm$ 0.0005	2.542 $\pm$ 0.155	0.0274 $\pm$ 0.0010	36.76 $\pm$ 0.59
	PolyCL	0.0519 $\pm$ 0.0022	0.0096 $\pm$ 0.0004	2.723 $\pm$ 0.247	0.0303 $\pm$ 0.0024	36.03 $\pm$ 0.93
	RDKit2D	0.0283 $\pm$ 0.0040	0.0071 $\pm$ 0.0004	3.471 $\pm$ 0.171	0.0235 $\pm$ 0.0014	33.33 $\pm$ 0.42
RDKit3D	0.1175 $\pm$ 0.0059	0.0202 $\pm$ 0.0006	4.354 $\pm$ 0.146	0.0406 $\pm$ 0.0017	73.38 $\pm$ 0.54	
TabPFN	MACCS	0.0305 $\pm$ 0.0052	0.0081 $\pm$ 0.0003	2.278 $\pm$ 0.265	0.0232 $\pm$ 0.0007	28.46 $\pm$ 0.49
	Mordred	0.0118 $\pm$ 0.0020	0.0051 $\pm$ 0.0004	1.877 $\pm$ 0.184	0.0156 $\pm$ 0.0004	23.09 $\pm$ 0.33
	Oligomer-Mordred	0.0109 $\pm$ 0.0018	0.0050 $\pm$ 0.0004	1.747 $\pm$ 0.220	0.0148 $\pm$ 0.0007	22.75 $\pm$ 0.36
	Oligomer-RDKit2D	0.0116 $\pm$ 0.0013	0.0052 $\pm$ 0.0004	1.921 $\pm$ 0.169	0.0160 $\pm$ 0.0003	23.10 $\pm$ 0.28
	PolyBERT	0.0246 $\pm$ 0.0018	0.0070 $\pm$ 0.0003	1.909 $\pm$ 0.149	0.0181 $\pm$ 0.0006	26.29 $\pm$ 0.38
	PolyCL	0.0213 $\pm$ 0.0021	0.0065 $\pm$ 0.0004	2.046 $\pm$ 0.129	0.0182 $\pm$ 0.0016	26.19 $\pm$ 0.88
	RDKit2D	0.0121 $\pm$ 0.0012	0.0053 $\pm$ 0.0003	2.002 $\pm$ 0.154	0.0171 $\pm$ 0.0004	23.59 $\pm$ 0.17
	RDKit3D	0.0646 $\pm$ 0.0043	0.0179 $\pm$ 0.0006	3.112 $\pm$ 0.178	0.0287 $\pm$ 0.0011	61.27 $\pm$ 0.83
FastKAN	RDKit2D	0.0146 $\pm$ 0.0010	0.0061 $\pm$ 0.0002	2.286 $\pm$ 0.195	0.0214 $\pm$ 0.0027	26.22 $\pm$ 1.02
FourierKAN	RDKit2D	0.0597 $\pm$ 0.0050	0.0108 $\pm$ 0.0003	3.151 $\pm$ 0.260	0.0296 $\pm$ 0.0022	36.93 $\pm$ 1.11
EfficientKAN	RDKit2D	0.0167 $\pm$ 0.0014	0.0066 $\pm$ 0.0001	2.254 $\pm$ 0.218	0.0211 $\pm$ 0.0019	28.71 $\pm$ 1.11
MLP	RDKit2D	0.0149 $\pm$ 0.001	0.0065 $\pm$ 0.0001	2.396 $\pm$ 0.0.264	0.021 $\pm$ 0.001	29.03 $\pm$ 0.77

## S4.2 Attempts on other models

In addition to the models discussed in the main text, we explored several alternative modelling strategies in this work. We report these results to provide additional insights for the polymer community on network design choices for polymer property prediction.

One approach is to explicitly incorporate polymer chain representations into the model. To construct a chain-level representation, we replicated the monomer embedding  $n$  times, where  $n$  denotes the polymer chain length. A reversal-invariant positional encoding is then applied to differentiate monomer positions along the chain. A class token is prepended to the sequence, and a three-layer Transformer encoder is used to update the monomer representations. We refer to this model as `gatv2_chain_readout`.

Another approach is motivated by the observation that atom ordering within a monomer is not strictly permutation-invariant due to the presence of attachment points. To account for this, we defined atom location features based on the shortest-path distance from each atom to the nearest attachment site. These location features are further encoded using positional encodings and added to the initial atom embeddings. This variant is denoted as `gatv2_pe`.

We also evaluated the Directed Message Passing Neural Network (DMPNN)<sup>S8</sup> as a representative message-passing baseline.

The performance of these three models is summarised in Table S21. The results indicate that `gatv2_chain_readout` yields improved performance for predicting  $R_g$ , which is consistent with the fact that  $R_g$  is inherently a chain-level property. The `gatv2_pe` model achieves performance comparable to, but not exceeding, that of the vanilla GATv2. DMPNN attains strong performance on density and TC; however, due to its substantially longer training time, experiments for FFV and  $T_g$  could not be completed within the allocated 72-hour time limit.

Table S21: Performance of additional GNN models on polymer property prediction (\* indicates that training was not completed within 72 hours).

Model	$\rho_{\text{md}}$	FFV	$R_g$	TC	$T_g$
GATv2	$0.0136_{\pm 0.0005}$	$0.0046_{\pm 0.0001}$	$1.7065_{\pm 0.0711}$	$0.0172_{\pm 0.0007}$	$22.4999_{\pm 0.7899}$
gatv2_chain_readout	$0.0166_{\pm 0.0010}$	*	$1.6924_{\pm 0.0852}$	$0.0186_{\pm 0.0018}$	*
gatv2_pe	$0.0143_{\pm 0.0007}$	$0.0048_{\pm 0.0002}$	$1.8040_{\pm 0.0953}$	$0.0181_{\pm 0.0026}$	$25.9572_{\pm 0.9894}$
DMPNN	$0.0114_{\pm 0.0006}$	*	$1.7144_{\pm 0.0926}$	$0.0157_{\pm 0.0019}$	*

### S4.3 Performance of empirical equations and atomic contributions

We estimated the target properties using empirical equations for the corresponding datasets (all sets) and evaluated their performance using parity plots against the ground-truth values (Figure S1). For density estimation, the Fedors and IBM group contribution methods perform well, achieving  $R^2$  values greater than 0.7. In contrast, among the atomic contribution methods, good performance is observed for  $T_g$ , whereas the predictions for TC and FFV are poor.

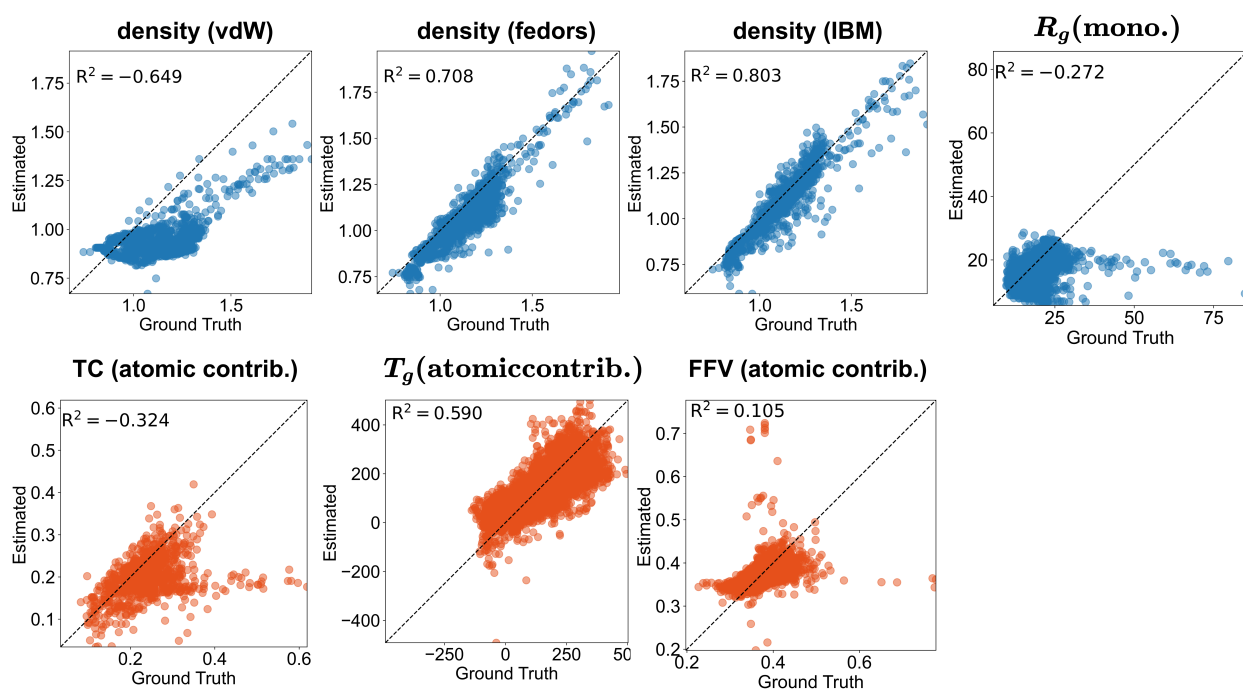


Figure S1: Performance of different empirical equations and atomic contribution methods.

## References

- (S1) Li, L.; Zhang, Y.; Wang, G.; Xia, K. Kolmogorov–Arnold graph neural networks for molecular property prediction. *Nat. Mach. Intell.* **2025**, *7*, 1346–1354.
- (S2) Xu, J.; Chen, Z.; Li, J.; Yang, S.; Wang, W.; Hu, X.; Ngai, E. C.-H. FourierKAN-GCF: Fourier Kolmogorov-Arnold Network—An Effective and Efficient Feature Transformation for Graph Collaborative Filtering. *arXiv preprint arXiv:2406.01034* **2024**,
- (S3) Li, Z. Kolmogorov-Arnold Networks are Radial Basis Function Networks. 2024; <https://arxiv.org/abs/2405.06721>.
- (S4) Xu, K.; Hu, W.; Leskovec, J.; Jegelka, S. How Powerful are Graph Neural Networks? International Conference on Learning Representations. 2019.
- (S5) Rampásek, L.; Galkin, M.; Dwivedi, V. P.; Luu, A. T.; Wolf, G.; Beaini, D. Recipe for a general, powerful, scalable graph transformer. Advances in Neural Information Processing Systems. 2022.
- (S6) Brody, S.; Alon, U.; Yahav, E. How Attentive are Graph Attention Networks? International Conference on Learning Representations. 2022.
- (S7) Hayashi, Y.; Shiomi, J.; Morikawa, J.; Yoshida, R. RadonPy: automated physical property calculation using all-atom classical molecular dynamics simulations for polymer informatics. *npj Comput. Mater.* **2022**, *8*, 222.
- (S8) Yang, K.; Swanson, K.; Jin, W.; Coley, C.; Eiden, P.; Gao, H.; Guzman-Perez, A.; Hopper, T.; Kelley, B.; Mathea, M.; Palmer, A.; Settels, V.; Jaakkola, T.; Jensen, K.; Barzilay, R. Analyzing Learned Molecular Representations for Property Prediction. *J. Chem. Inf. Model.* **2019**, *59*, 3370–3388.